LLNL-JRNL-2003787

Paleoclimatic implications of glacial fluctuations in the Sierra Nevada del Cocuy, Northern Andes, Colombia, during the Lateglacial and Ho...

G Bromley, J Herbert, S Londoño, A Hidy, M Kelly, A Doughty, S Restrepo-Moreno, P Galloway

June 2025

This work performed under the auspices of the U.S. Department of Energy by Lawrence Livermore National Laboratory under Contract DE-AC52-07NA27344.

Paleoclimatic implications of glacial fluctuations in the Sierra Nevada del Cocuy, Northern Andes, Colombia, during the Lateglacial and Holocene

Jordan N. Herbert[1], *Gordon R.M. Bromley[2,3], Meredith A. Kelly[1], Alice M. Doughty[4], Daniel Ruiz-Carrascal[5], Sergio A. Restrepo-Moreno[6,7], Santiago Noriega Londoño[8], Peter Galloway[1], Alan J. Hidy[9]

[1]*Department of Earth Sciences, Dartmouth College, Hanover, NH 03755, USA*
[2]*Geography, University of Galway, Galway H91 TK33, Ireland*
[3]*Climate Change Institute, University of Maine, Orono, ME 04469, USA*
[4]*School of Earth & Climate Sciences, University of Maine, Orono, ME 04469, USA*
[5]*Innovation and Technological Development Directorate, EAFIT University, Medellín, Colombia*
[6]*Departamento de Geociencias y Medio Ambiente, Universidad Nacional de Colombia, Medellín, Colombia*
[7]*Department of Geological Sciences, University of Florida, Gainesville, FL 32611, USA*
[8]*Grupo de Estudios Tectónicos, Departamento de Medio Ambiente y Desarrollo, Universidad Nacional de Colombia, Medellín, Colombia*
[9]*Center for Accelerator Mass Spectrometry, Lawrence Livermore National Laboratory, Livermore, CA 94550, USA*
*Corresponding author

Highlights:

- Relict moraines in the northern Colombian Andes reveal changes in tropical air temperature over the last ~16,000 years.
- Colombian glaciers advanced during the Antarctic Cold Reversal and retreated during the Younger Dryas period, similar to the broader tropical pattern of cryospheric change.
- Lateglacial climate shifts are potentially linked to ocean-atmosphere heat transfer and atmospheric vapor flux.
- The magnitude of Lateglacial temperature shifts are minor relative to modern warming.

Keywords: Lateglacial, Holocene, Glacial, Geomorphology, Quaternary, Tropics, Andes, Colombia, Cosmogenic Beryllium-10

Abstract: The reconstruction of former mountain glaciers from geomorphic mapping and cosmogenic-nuclide surface-exposure dating provides a unique opportunity to infer patterns of past terrestrial climate variability. Tropical mountain glaciers are particularly valuable as there are comparatively few terrestrial climate proxies at equatorial latitudes relative to higher latitudes. As the single largest climate zone on Earth, the tropics play an outsized role in mediating global climate via the ocean-atmosphere transfer of latent heat and water vapor. Nonetheless, there remains a persistent gap in our understanding of how the tropics influenced – or were influenced by – the high-magnitude climate shifts of the Late Pleistocene, and whether this high-energy region simply responded to extratropical forcing or was itself a driver of global climatic change. To help address this knowledge gap, we analyzed geologic evidence for past glacial fluctuations in three adjacent valleys in the Sierra Nevada del Cocuy, the highest subrange of the Eastern Cordillera in the Colombian Andes, to provide a terrestrial record of atmospheric temperature during the latter part of Termination 1. Coupled with geomorphic mapping and paleo-snowline reconstructions, our beryllium-10 glacial chronology indicates that glaciers in the humid inner tropics underwent pronounced growth and gradual decay during the Antarctic Cold Reversal and Younger Dryas periods, respectively, following a trend that, according to directly dated moraine records from throughout both polar hemispheres, appears to have been global. While the specific mechanism(s) behind this large-scale behavior remains to be corroborated, we revisit the hypothesis that ocean-atmosphere heat transfer and water vapor flux are key drivers of abrupt Lateglacial temperature fluctuations. Subsequent to the Lateglacial, deglaciation of the Sierra Nevada del Cocuy accelerated during the Early Holocene, a pattern also observed in other tropical glacier records. More recently, the magnitude of snowline rise and glacier retreat over the last two centuries supports the view that modern tropospheric warming is anomalously strong at least relative to the last ~16,000 years.

1. Introduction

The tropics (23.5°N–23.5°S) are the primary source of heat energy and water vapor for Earth's climate system (Seager and Battisti, 2007; Chiang, 2009) and, as such, have the potential to propagate climatic perturbations rapidly and globally. Yet our understanding of the tropical role in ice age cycles and abrupt climate change is far from complete, reflecting the relatively low spatial coverage of detailed paleoclimate records from equatorial latitudes. This dearth of information is particularly acute at higher elevations, where recent assessments suggest the magnitude of tropospheric temperature change is amplified by moisture-driven fluctuations in the lapse rate (Loomis et al., 2017; Garelick et al., 2022; Legrain et al., 2023). Compounding the problem further, the geographic distribution of tropical paleoclimate datasets is far from uniform, precluding accurate assessment of any latitudinal climate variability. For example, the tropical Andean glacial-geologic record for the last glacial period is heavily skewed towards the Southern Hemisphere (e.g., Bromley et al., 2009, 2011, 2016; Martin et al., 2020; Rodbell et al., 2009; Shakun et al., 2015; Smith et al., 2005), while the northern tropical Andes are represented by only a handful of studies (e.g., Carcaillet et al., 2013; Jomelli et al., 2014; Angel et al., 2016; Stansell et al., 2010). Our new record from Cocuy thus helps address a persistent gap in our understanding of Lateglacial terrestrial temperature in the northern tropics.

Glaciers are highly sensitive indicators of mean climate conditions (Oerlemans, 1989), and reconstructions of past glacier behavior provide some of the clearest evidence for tropical terrestrial climate variability (e.g., Jomelli et al., 2014). If sufficiently well-dated, such geologic records can be used to test new hypotheses surrounding the mechanisms and spatial impact of millennial-scale climate shifts during the last glacial-interglacial transition, known as Termination 1 (~19–11 ka). Our study is motivated by the need for robust tropical glacial chronologies from both polar hemispheres to assess the geographic extent and plausible mechanisms of millennial-scale climatic shifts during Termination 1.

Recent refinement of cosmogenic nuclide production rates in low-latitude, high-altitude applications (Blard et al., 2013; Kelly et al., 2015; Martin et al., 2015) has greatly improved our ability to date tropical glacial records directly and accurately, thereby providing a critical foundation for comparing tropical paleoclimate data with global records. An attendant issue relating to the use of glacier extents as paleoclimate proxies is whether factors other than climate influence glacial configuration and moraine deposition (e.g., Barr and Lovell, 2014). This is particularly important in the tropics, where glaciers are relatively small (typically <1 km^2) and thin (<100 m) and, thus, potentially more sensitive than larger glaciers to topographic influences such as headwall height, valley slope, and accumulation-area topography. A means to assess the influence of topography on glacial extents is to develop and compare detailed records for multiple glacial extents within a single area, for which climate conditions are relatively homogenous. Most tropical mountain ranges are geographically compact and thus provide an ideal setting for examining similarities and differences among multiple paleo-glacial systems.

In this paper, we compare moraine sequences corresponding to the Lateglacial period of Termination 1 in three valleys of the Sierra Nevada del Cocuy (hereafter 'Cocuy'), Colombian Andes. By reconstructing changes in glacier equilibrium-line altitude (ELA) for each dated paleo-glacier, we estimated the magnitude of Lateglacial temperature change at Cocuy. The result is a new terrestrial record of tropospheric temperature from the northern Andes, which we use to evaluate the relative timing and magnitude of key climate events within the tropics and globally. Further, by comparing past glacier behavior in multiple adjacent catchments, we make a preliminary examination of the topographic role in glacier configuration and, therefore, moraine deposition. By identifying similarities among the multiple glacial systems, we have extracted climatic information that cannot be drawn from a single valley or a limited number of landforms (Balco, 2020).

2. Geologic and climatic setting

Positioned close to the northern limit of the tropical Andes, the Sierra Nevada del Cocuy (6.44° N, 72.29° W; Fig. 1) in the Eastern Cordillera is the highest sub-range of three Colombian cordilleras (Western, Central, and Eastern) and culminates in the 5490 m asl summit of Ritacuba Blanco. Centered on the cordillera's syntaxial bend, where significant local relief develops over an antiformal lobe (Kammer et al., 2020), Cocuy constitutes one of the main foci of crustal deformation and topographic build-up during the late Miocene's Eu-Andina orogenetic phase (Restrepo-Moreno et al., 2019). The structural orientation of the underlying Cretaceous sedimentary lithologies (primarily resistant layers of white quartzose sandstone and conglomeratic sandstones of the Une-Aguardinete Formation), which are arranged in thick strata with a general dipping trend of 20–25° to the west (Fabre et al., 1984), results in an asymmetric sierra-like topography at Cocuy, whereby low-gradient surfaces forming the western slopes contrast with precipitous slopes forming the eastern flanks (Mendivelso, 2016); this orientation plays a key role in local patterns of glaciation (see below).

Today, Cocuy hosts approximately 12 of the remaining non-volcanic glacial summits in Colombia. Over the last five decades, the aerial extent of Cocuy's total glacier cover has declined from ~30 km^2 in 1987 to ~15 km^2 in 2019 (López-Moreno et al., 2022; Molano et al., 2022). Climatically, Cocuy is positioned in the inner tropics and as such experiences high year-round humidity; precipitation (~1270 mm rain annually: Sturm and Rangel, 1985) is derived primarily from the Atlantic Ocean via the prevailing easterly airflow (Masiokas et al., 2020) and maximum precipitation coincides with the spring and autumn passage of the Inter Tropical Convergence Zone (ITCZ) (Masiokas et al., 2020; Rabatel et al., 2013). During the period 2007–2016, the average 0°C isotherm in the Cordillera Oriental was at ~5050 m asl (Rabatel et al., 2017), marginally higher than earlier estimates of Cocuy glacier ELAs (4700–4900 m asl) based on mass balance measurements (Helmens et al., 1997; Lachniet and Vazquez-Selem, 2005). Further, modern variability in tropical freezing level height, and therefore glacier behavior, has been linked directly to changes in equatorial Pacific sea surface temperatures (SSTs) (Bradley et al., 2003; Rabatel et al., 2013; Ruiz-Carrascal et al., 2022).

In this study, we focus on the Lagunillas valley and one of its major tributaries, the Bocatoma valley, located in the southern portion of Cocuy, and compare those results with the moraine record from the Cardenillo valley on Ritacuba Negro, 15 km north of our site (Jomelli et al., 2014, 2017) (Fig. 1). Lagunillas forms a broad south-to-north-oriented catchment draining the southwestern side of the range for 15 km, where it joins the Río Cóncavo at 3290 m asl. In its lower, northern half, the Lagunillas valley is relatively narrow and hemmed in by steep, densely vegetated valley walls; the latter include the proximal slopes of high-relief Late Pleistocene lateral moraines. Approximately 8 km up-valley from the Cóncavo confluence, the Lagunillas becomes a lower gradient, broader valley (mean slope ~7%) characterized by moraine-dammed wetlands and open páramo vegetation, with a southern limit marked by a ~4500 m-high bedrock ridgeline. The Río Bocatoma drains the Pan de Azúcar glacier and enters the Lagunillas valley from the east immediately downstream of Laguna La Pintada (Fig. 2). In contrast to Lagunillas, Bocatoma exhibits a steep profile (mean ~20%), dropping 750 m over a distance of <4 km and constrained throughout by precipitous rock walls (Fig. 3). Completing this study, the Cardenillo valley drains the glaciated western flank of Ritacuba Negro at the northern end of the range (Jomelli et al., 2014) (Fig. 1). Ritacuba Negro currently supports the range's most extensive glacier cover (~3.3 km^2) between ~4750 m asl and the summit at 5350 m asl. Between ~3960 and 4300 m asl, where the moraines investigated by Jomelli et al. (2014) are located (Fig. 4), the Cardenillo valley assumes a broad glacial U-shape form with a gentle longitudinal profile (mean 7%) and low-gradient valley walls; these topographic characteristics are typical of the main glaciated catchments at Cocuy. Above 4300 m asl, the drainage becomes both broader and steeper (~20%), with ice-free portions of the hillside dominated by bare, glacially molded bedrock.

Owing to their relative proximity to one another, we anticipate that our three target glacier systems experienced similar climatologic conditions during the Late Pleistocene. Moreover, the dominant lithology at all three sites is quartzose sandstone (quartz arenite), and thus ideal for ^{10}Be surface-exposure dating.

3. Prior glacial-geologic research at Cocuy

Previous work on the paleoclimatology of Cocuy spans six decades, during which past environmental conditions have been inferred from radiocarbon-dated pollen assemblages, sedimentology, and expansive mapping of glacial geomorphology (Gonzalez et al., 1965; Helmens et al., 1997; Kuhry et al., 1993; van der Hammen et al., 1980; van der Hammen and Hooghiemstra, 1995). All prior radiocarbon ages described below have been calibrated via the CALIB Radiocarbon Calibration program v8.2html and the IntCal20 dataset (Reimer et al., 2020). During the first such investigations in the study area, Gonzalez et al. (1965) and van der Hammen et al. (1980) established pollen chronozones from lake and bog sediments retrieved from the Lagunillas and Bocatoma valleys. Those authors inferred that the coldest conditions of the last ~48 kyr occurred prior to 25 ka, with cool, dry climate persisting during the period 25–17 ka (Gonzalez et al., 1965; van der Hammen et al., 1980). According to existing interpretations of the pollen record, subsequent climate warming between ~17 and 15.6 ka was followed by cooling at ~15.6–14.7 ka, after which warming resumed at ~14.7 ka (Kuhry et al., 1993; van der Hammen et al., 1980). Finally, the *El Abra* stadial was interpreted as a cool tropical equivalent to the Younger Dryas stadial (van der Hammen and Hoogheimstera, 1995).

Building on the initial geomorphologic work of Gonzalez et al. (1965), van der Hammen et al. (1980) reported six discrete glacial drift units (Drifts 1–6, from oldest to youngest) preserved throughout the range and assigned these to specific glacial stages on the basis of elevation, relative weathering, and vegetation development. While the oldest unit, Drift 1, is spatially and temporally undifferentiated, a calibrated basal radiocarbon age of 25.1 ± 0.4 cal ka BP (GrN 6907: 20,840 ± 140 ^{14}C yr BP) from Laguna Ciega (3510 m asl), near the village of Guicán (Fig. 1), provides minimum-limiting constraint for the overlying Drifts 2 and 3 (van der Hammen et al., 1980). On this basis, van der Hammen et al. (1980) concluded that Drifts 2 and 3 correspond to glacial advances that predated the Last Glacial Maximum (LGM: ~26–19 ka). Since these drift units predate Termination 1, we do not discuss these deposits further in this paper.

The Drift 4 type area is the Lagunillas valley, where van der Hammen et al. (1980) reported multiple well-preserved moraine sets corresponding to the last glacial cycle and Termination 1. Within the upper Drift 4 sequence, at an elevation of 3880 m asl, Gonzalez et al. (1965) reported a river-cut section in which laminated muds and organic sediments are exposed (section VL-V: 3880 m asl; Figs. 1, 3A). Those authors correlated this paleo-lacustrine unit with glacial meltwater from the subsequent Drift 5 episode; if so, a radiocarbon date of 12,320 ± 100 ^{14}C yr BP (GrN 3247: 14.4 ± 0.4 cal ka BP) from the unit provides both a minimum-limiting age for the Drift 4 deposits and a maximum-limiting age for the Drift 5 moraines (Gonzalez et al., 1965).

Drift 5 was described by van der Hammen et al. (1980) as comprising "fine, high, broad and curved bordering moraines" marking former ice-terminal positions, the lowermost of which lies at ~3900–4200 m asl. In the Lagunillas valley, van der Hammen et al. (1980) mapped these deposits solely in relation to the former Bocatoma glacier, which terminated on the Lagunillas valley floor at 3950 m asl (Figs. 2, 3) and reportedly provided the fine-grained sediments exposed in the VL-V section (Gonzalez et al., 1965). Farther north, van der Hammen et al. (1980) also correlated Drift 5 with the large lateral moraine complex preserved in the Cardenillo valley on Ritacuba Negro (Fig. 4), the focus of a more recent study by Jomelli et al. (2014).

According to van der Hammen (1980), the lowermost moraines preserved in the Cardenillo valley correspond to Drift 4 and occur as isolated, low-relief ridge sections and mounds at approximately 3960 m asl. Half a kilometer up-valley from the proposed Drift 4 limit, a set of three well-defined left-lateral moraines marks the former extent of the Ritacuba Negro glacier at some as-yet undetermined time during the Late Pleistocene. The left-lateral complex is traceable for ~2 km as it rises along the southern valley wall, before becoming indistinct at 4275 m asl. In contrast, the equivalent right-lateral moraines are discontinuous and less clearly defined. For approximately one kilometer upslope of this former glacier position, a series of lower-relief (<10 m high) lateral-terminal ridges marks successive stages of a thinner ice tongue that terminated between ~3900 and 4000 m asl (Fig. 4), and which includes moraines M16, M17, and M18 as mapped by Jomelli et al. (2014). Those authors reported mean ^{10}Be ages for the M16–M18 moraines of between 14.0 ± 0.3 and 13.4 ± 0.3 ka.

This Lateglacial suite is overlain in turn by a conspicuous complex of boulder-covered moraine ridges that van der Hammen et al. (1980) assigned to their Drift 5, and which Jomelli et al. (2014) ^{10}Be dated to between 11.8 ± 0.3 and 11.1 ± 0.3 ka (moraines M13–M15; Fig. 4). This complex is relatively massive, towering ~80 m above the valley bottom and comprising >10 arcuate moraines. Enclosed by this complex is a small, fluvially incised wetland in which several discontinuous moraine fragments mark recessional stages of the Ritacuba Negro glacier (Jomelli et al., 2014). The youngest and highest glacial deposit mapped by van der Hammen, Drift 6, is characterized by conspicuous, unweathered moraines with minimal vegetation cover, and marks the most recent widespread glacial advance. In the Cardenillo valley, five ^{10}Be ages from unweathered moraines confirm that Drift 6 is Late Holocene in age (moraines M4 and M12; Jomelli et al., 2014).

The rich Quaternary stratigraphy preserved at Cocuy has the potential for providing directly dated geological records of past climate variability in the humid inner tropics and for placing modern climate change in a longer-term context. Advancing from this foundation, the remainder of this paper reports the glacial-geologic perspective on the Lateglacial period of Termination 1; the LGM and early Termination 1 portions of the record are the focus of a subsequent paper. As part of the current study, we report the recalculated ages of Jomelli et al. (2014) for comparison with our new data.

4. Methods

4.1 Glacial-geomorphic mapping based on remote sensing and field observations

We constructed glacial-geologic maps for our target valleys: upper Lagunillas and Bocatoma (Fig. 5). For both, we first used Google Earth imagery to draft preliminary glacial-geologic maps, which served subsequently as guides during our fieldwork in 2012, 2018, and 2023. We then drafted geomorphic maps using QGIS coupled with satellite imagery derived from the Centre National d'Etudes Spatiales (image date 17 December, 2017) and the 12.5 m-resolution Alos Palsar digital elevation model. Each map includes key glacial depositional features and contextual non-glacial features (e.g., lagoons, rivers). Our assessment of the Cardenillo valley is based solely on remotely sensed imagery and the prior survey-based mapping of Jomelli et al. (2014, 2017).

4.2 Beryllium-10 surface-exposure dating

We sampled moraines in the Lagunillas and Bocatoma valleys for cosmogenic ^{10}Be surface-exposure dating, targeting large, stable quartz arenite boulders located on moraine crests to minimize the potential influences of post-depositional movement and shielding by sediment, snow, or vegetation (Balco, 2011) (Fig. 6). We also collected samples from boulders and bedrock located immediately outside moraine ridges to provide broader temporal context for moraine formation. We processed 36 samples from Lagunillas and Bocatoma valleys (Table 1). In the University of Galway's Palaeoenvironmental Research Unit, we isolated quartz from the whole-rock samples using heavy-liquid density, magnetic separations, and progressive leaching in hydrofluoric/nitric acid. In the laboratory at Dartmouth College, we spiked samples using a beryllium 9 carrier made from a deeply buried beryl crystal and used ion chromatography to extract beryllium from the pure quartz, following methods modified from Schaefer et al. (2009). We measured ^{10}Be/^{9}Be ratios of the samples at the Center for Accelerator Mass Spectrometry, Lawrence Livermore National Laboratory.

In total, we processed six batches of samples, with one process blank per batch; blank corrections were made by calculating the number of ^{10}Be in the blank and subtracting this number from each sample in the respective batch. Blank ^{10}Be/^{9}Be ratios range between 9.95×10^{-17} and 2.53×10^{-16}, representing < 2% (and typically < 1%) of the ratio for each sample measured, and sample measurement errors are 1.6–2.2% (Table 1). To calculate surface-exposure ages from ^{10}Be concentrations, we used version 3 of the UW online calculator (https://hess.ess.washington.edu/math/v3/v3_age_in.html) in conjunction with the Quelccaya ^{10}Be production rate (Kelly et al., 2015). All input data and production rate data for this calculator are provided in Table S1. This production rate was calibrated against ^{14}C–dated moraines in the Peruvian Andes, in a similar geomagnetic and geographic setting as Cocuy, and thus we consider it to be appropriate for this study. Below, we discuss ^{10}Be ages calculated using the time-invariant ("St") scaling of Lal (1991) and Stone (2000); we also report ^{10}Be ages determined using other scaling methods (e.g., "Lm" (Lal, 1991; Stone, 2000; Nishiizumi et al., 1989) and "LSDn" (Lifton et al., 2014)) in Table 2. For consistency, we recalculated published ^{10}Be ages from the Cardenillo valley with the same production rate and scaling methods (Tables 2 and S1; Fig. 4).

We report individual ^{10}Be ages with both their respective internal errors, reflecting accelerator mass spectrometry (AMS) measurement uncertainties, and external errors, which includes the systemic production rate uncertainty (Table 2). For landforms with two or more ^{10}Be ages, we calculated both the mean and peak ages to establish the likeliest landform age. Further, for each population, we calculated the standard deviation of the mean and the reduced weighted mean uncertainty, and applied the larger of the two as our reported age uncertainty. We identify ^{10}Be ages that are outliers on moraines using a reduced chi-squared analysis (Balco, 2011) and considering the stratigraphic order of moraines. Since the surface-exposure age of a boulder on a moraine represents the final occupation of that position by ice, we interpret moraine ages as indicating the onset of moraine abandonment due to glacier retreat.

4.3 ELA and paleo-temperature reconstruction

Glacier mass balance is influenced by both temperature (energy) and precipitation (mass). In the humid inner tropics, where precipitation remains relatively stable year-round, glacier mass balance is dominated by the availability of energy for melting ice (Kaser and Osmaston, 2002; Taylor et al., 2006; Rupper and Roe, 2008; Sagredo et al., 2014). Accordingly, fluctuations in past glacier (‘paleo-glacier’) length at Cocuy are a first-order indication of air temperature variability (ΔT). For a glacier in equilibrium with climate, the steady state ELA is the average elevation at which annual accumulation is equal to annual ablation (Porter, 2001; Benn et al., 2005). Thus, comparing the ELAs of former glacial extents, reconstructed from relict moraines, affords a powerful tool for interpreting past climate change.

We used the ArcGIS toolboxes provided by Pellitero et al. (2015, 2016) to calculate paleo-ELA values for former glacier extents at Cocuy. This approach first reconstructs the paleo-glacier surface following the model outlined in Benn and Hulton (2010) and then calculates ELAs for the paleo-glacier surface reconstruction using the accumulation-area ratio (AAR) and area-altitude balance ratio (AABR) methods. For the modeling element, we reconstructed paleo-glaciers for each dated moraine using a standard basal shear stress value of 100 kPa (Benn and Hulton, 2010; Pellitero et al., 2016). We traced each mapped moraine extent in ArcGIS and established the catchment of former accumulation areas with the ArcGIS Spatial Analyst.

The AAR method assumes a glacier's accumulation area occupies a calculable proportion of the total glacier area (Porter, 2000), which in turn depends on such factors as lapse rate and glacier hypsometry (Benn et al., 2005). Whereas temperate glaciers typically exhibit AARs of ~0.6, this value is higher in the tropics due to the absence of thermal seasonality; glaciers undergo year-round ablation and thus require larger accumulation zones to balance mass loss (Kaser and Osmaston, 2002). Idealized simulations of tropical AARs (0.82: Kaser and Osmaston, 2002) are similar to the optimal AAR (~0.80) reported by a recent analysis of nine paleo-glaciers in the Venezuelan Andes (Stansell et al., 2017). The AABR method also incorporates glacier mass-balance and hypsometry and is considered more representative of the true glacier ELA (Benn et al., 2005; Kaser and Osmaston, 2002). Balance ratios (BRs, used in the AABR method) for mid-latitude glaciers typically are in the range 1.8–2.2 (Benn and Lehmkuhl, 2000; Rea, 2009); tropical BRs are generally higher, reflecting the larger AARs (Rea, 2009), with values as high as 25 reported for some tropical systems (Benn and Evans, 1998). We present ELAs calculated with a range of plausible AARs and BRs in Table 3.

We quantified ΔT for each dated moraine extent by comparing a paleo-ELA to a reference ELA and applying an appropriate lapse rate to the offset. This method assumes that glacial fluctuations are primarily a response to changes in atmospheric temperature, with precipitation playing a relatively minor role. This first-order relationship is confirmed for the humid inner tropics by studies of extant and former glaciers, which highlight the impact of high year-round precipitation on glacier mass-balance gradients and, thus, thermal sensitivity (Benn et al., 2005; Favier et al., 2004; Hastenrath, 2009; Rupper and Roe, 2008; Sagredo et al., 2014). A second variable in deriving ΔT from ΔELA is the atmospheric lapse rate. Today, inner tropical environments at elevations <5000 m asl generally experience a moist adiabatic lapse rate of approximately 5.5°C/km (Loomis et al., 2017), significantly lower than the global mean environmental lapse rate (6.5°C/km) (Barry and Chorley, 2003). Prior estimates based on meteorological data suggest modern lapse rates for Colombia of ~5.7°C/km (DeForest Safford, 1999; Sturm and Rangel, 1985), although some studies reported values closer to 6.5°C/km for the Cocuy region (Kuhry et al., 1993; van der Hammen and Gonzalez, 1960).

Recent alkenone paleothermometry from tropical African lakes documents a lapse rate during the LGM (6.7 ± 0.3°C/km) that was considerably steeper than at present (5.8 ± 0.1°C/km) (Loomis et al., 2017; Garelick et al., 2022). To date, however, no similar studies have been conducted in South America. Evaluating ELA reconstructions from Venezuela, Stansell et al. (2007) suggested that the LGM lapse rate for the northern Andes could have been moderately steeper than present, whereas pollen-inferred estimates are inconclusive (Bakker, 1990; Farrera et al., 1999). Acknowledging this uncertainty, we follow the approach of Stansell et al. (2007) and employ a range of lapse rates between 5 and 7°C/km in our ELA-based estimates of ΔT. For a reference ELA, we used the 1955 CE values for the Pan de Azúcar and Ritacuba Negro glaciers reported by López-Moreno et al. (2022) based on aerial photography from that year (Agustín Codazzi Geographic Institute) (Table 3). Since the Lagunillas valley is too low to have supported Late Holocene glaciers, we employed the adjacent Pan de Azúcar value (Table 3) as a reference ELA for this catchment. We take the 1955 CE glacial configuration as representing Cocuy temperatures prior to significant anthropogenic warming.

5. Results

5.1 Glacial geomorphology

Following retreat from the Drift 4 moraines located farther down-valley (van der Hammen et al., 1980), the Lagunillas system separated into two distinct glaciers: a north-flowing system occupying the upper Lagunillas valley above Laguna La Pintada (3960 m asl) and a west-flowing tongue draining Pan de Azúcar via the Bocatoma valley (Fig. 2). In this section, we first describe the upper Lagunillas stratigraphy before reporting on the Bocatoma stratigraphy; the glacial stratigraphy of the Cardenillo valley was reported previously by Jomelli et al. (2014).

Lagunillas valley

Immediately south of Laguna La Pintada, the broad valley bottom is dominated by ice-molded bedrock overlain with a thin, patchy till cover and perched glacial boulders. Within 200–600 m of the lagoon, however, and damming Laguna Cuadrada, a suite of well-preserved prominent terminal and lateral moraine ridges defines the former terminus of the Lagunillas glacier during the culmination of a significant advance. The complex comprises three principal ridges (hereafter termed the Pintada moraines; Fig. 2) that, despite their moderate relief (2–10 m), are conspicuous in their uniformity of form and their lateral continuity. The outer ridge can be traced for almost 2 km as it crosses the corrugations of the valley floor between 4020 and 4070 m asl (Figs. 2, 5). Ridge crests are mantled with quartz arenite boulders, many of which exhibit clear morphological evidence for subglacial molding. Proximal to the Pintada moraines, more than 30 well-defined ridges, themselves forming five broad groupings, describe the active southward (up-valley) retreat of the Lagunillas ice margin over ~2.5 km (Figs. 2, 5); the highest of these recessional moraines is located at ~4200 m asl. All moraines investigated in the upper Lagunillas catchment exhibit similar degrees of soil development, vegetation cover, and relatively minor boulder surface weathering; several impound sizeable lakes (Fig. 3).

Bocatoma valley

Today, ice in the Bocatoma drainage is restricted to elevations above 4730 m asl on the southwestern slopes of Pan de Azúcar (Figs. 2, 6). During Lateglacial times, however, the Bocatoma glacier constructed an extensive complex of prominent, high-relief lateral moraines and well-preserved arcuate terminal ridges on the floor of the Lagunillas valley, immediately north of the moraine-impounded Laguna La Pintada (Fig. 2). Our investigation revealed that, rather than one single complex, the lower Bocatoma moraines form two discrete sequences (Fig. 2), with markedly different physical characteristics. The outer sequence, which we refer to as the Sisuma moraines, comprises five terminal moraine sections. These moraines are typically 2–4 m in relief and exhibit broad, vegetated crests with sparse quartz arenite boulders. Boulder surfaces are moderately pitted and exfoliated. Unlike the inner suite, the outer moraines lack significant lateral components, these presumably having been removed by the Río Lagunillas. Moreover, the most distal terminal ridges in this suite are partially obscured by colluviated till on the western valley side.

The inner sequence is dominated by a well-defined terminal moraine, located immediately west of the river channel, and a pair of high-relief composite lateral moraines emanating from the Bocatoma valley (Figs. 2, 3). In keeping with van der Hammen et al. (1980), we refer to these Drift 5 deposits as the Bocatoma moraines. The terminal moraine is 2–3 m tall on its distal side but as much as 4–5 m tall on the proximal side, where it has been incised by fluvial action. The crest is broad and moderately vegetated, with a concentration of large (>2 m diameter) quartz arenite boulders mantling the southern half of the landform. Below the surface, recent excavations have exposed glacio-tectonized units of laminated blue-gray clay (Fig. 6), indicating that the moraine is at least partially constructed of reworked lacustrine sediments and, thus, was formed by a glacier readvance. Inboard of the principal terminal ridge, a series of lower-relief bouldery moraines marks the active eastward retreat of the glacier terminus into the Bocatoma valley itself, at the mouth of which a bouldery arcuate terminal moraine at ~4025 m asl marks the final period of deposition in this complex (Figs. 3, 5). The Bocatoma terminal moraine sequence spans ~80 m in elevation over a distance of ~400 m, making it by far the steepest transect in this study. Flanking the terminal moraines, the sharp-crested lateral ridges exhibit a maximum relief of 50 m and can be traced for over a kilometer east of the former terminus (Figs. 2, 5), until they become indistinct at ~4260 m asl.

Upvalley of the prominent Bocatoma landforms, two sets of relatively subdued bouldery moraines, the lower at ~4090 m asl and the upper at ~4130 m asl, are separated by a peat wetland and mark subsequent stages of glacial deposition within the valley (Figs. 2, 5). The moraines of each unit have a vegetation cover similar to the Bocatoma moraines, while the constituent boulder surfaces are similarly pitted and exfoliated. An abrupt transition occurs at 4200 m asl, where the vegetated moraines have been overlain by relatively fresh, sparsely vegetated deposits corresponding to Drift 6 of van der Hammen et al. (1980) (Fig. 3). At the time of writing, the ice margin at the head of the Bocatoma catchment was located on bare molded bedrock at ~4600 m asl on the southern flanks of Pan de Azúcar.

5.2 Beryllium-10 moraine chronologies

Lagunillas valley

We ^{10}Be dated 18 boulders located on moraines in the upper Lagunillas valley (Fig. 5; Tables 1, 2). Ten samples from the three closely spaced Pintada moraines yield ages ranging from 13.2 ± 0.2 to 13.9 ± 0.3 ka (Fig. 5); an additional sample from the outer moraine (SNC-12-02: 15.1 ± 0.4 ka) returned an age >2σ beyond the mean and is rejected as an outlier. While the oldest sample in our dataset (SNC-12-03: 13.9 ± 0.3 ka) is from the outer crest, there is no significant age difference among the three moraines and, thus, we consider them as a unit, with mean and peak ages of 13.7 ± 0.4 ka and 13.6 ka, respectively (Fig. 5). Immediately down-valley (north) of the Pintada moraines, two distal boulders located on the indistinct crests of low-relief (~1 m tall) recessional moraines give ages of 15.6 ± 0.3 and 16.3 ± 0.3 ka and constrain the time of deglaciation prior to deposition of the Pintada complex (Fig. 5). As this deposit corresponds stratigraphically to the Sisuma moraines, so we refer to the unit collectively as Sisuma drift. Approximately 0.5 km up-valley of the Pintada moraines, an age from the prominent moraine bounding Laguna Cuadrada to the south yielded an age of 9.4 ± 0.2 ka (SNC-12-08: Fig. 5; Table 2); this age is out of stratigraphic order with the younger moraines farther up-valley and we reject it as an outlier. An age from the moraine south of Laguna La Atravesada suggests abandonment of this limit at 11.6 ± 0.2 ka, while three boulders on the uppermost prominent moraine in the valley, adjacent to Laguna La Parada, yielded mean and peak ages of 11.4 ± 0.1 ka and 11.4 ka, respectively (Fig. 5).

Bocatoma valley

Four boulder samples on the largest and innermost Sisuma moraine crest yield ^{10}Be ages ranging from 16.1 ± 0.3 to 17.1 ± 0.3 ka, with mean and peak ages of 16.6 ± 0.4 ka and 16.7 ka, respectively (Fig. 5). A fifth sample is 15.2 ± 0.3 ka, which is sufficiently younger than the main population to be considered an outlier. Inboard of the Sisuma moraines, six boulders on the large outer Bocatoma terminal moraine are 12.1 ± 0.2 and 13.3 ± 0.2 ka, with mean and peak ages of 12.7 ± 0.4 ka and 12.6 ka, respectively (Fig. 5). Three samples of boulders on the inner Bocatoma terminal moraine range from ~10.9 to 11.5 ka (mean 11.2 ± 0.3 ka; peak 11.3 ka) (Fig. 5).

To place the Bocatoma complex within a broader temporal context, we also ^{10}Be dated samples from higher elevation in the valley. A single boulder embedded in a minor recessional ridge at 4180 m asl, ~1 km up-valley of the inner Bocatoma terminal moraine, yielded an age of 10.7 ± 0.2 ka (SNC-12-12) (Fig. 5); stratigraphically, this vegetated landform is part of Drift 5 of van der Hammen et al. (1980). Within 90 m of that sample, two boulders located on the outer ridge of the overlying fresh deposits returned ages of 340 ± 10 and 620 ± 15 years (mean 0.5 ± 0.2 ka) (Fig. 5; Table 2). Finally, a single sample comprising striated, ice-molded bedrock collected from within 2 m of the 2012 ice margin returned an exposure age of ~30 ± 5 years (Fig. 5). We note this value is statistically indistinguishable from a subsequent measurement of quartz from the same sample reported by Gorin et al. (2024).

Cardenillo valley

Jomelli et al. (2014, 2017) determined forty-six ^{10}Be ages of boulders on eight moraines in the Cardenillo valley. We recalculated their ages using the same production rate and scaling scheme as for our own data, and report those recalculated ages in Table 2 and Figure 4. The recalculated ages differ from the originally published values by <1%. All samples marked as statistical outliers were identified as such by the original authors. Five recalculated ages from the outermost sampled moraine ('M18' of Jomelli et al., 2014) range between 12.8 ± 0.8 and 14.6 ± 0.4 ka (mean 13.8 ± 0.3 ka; peak 14.5 ka) (Fig. 4; Table 2), while the next sampled moraine ('M17') returns four recalculated ages between 13.8 ± 0.8 and 14.4 ± 0.7 ka (mean 14.1 ± 0.1 ka; peak 14.1 ka). According to Jomelli et al. (2014), the 'M16' moraine comprises two separate ridges, one located on the southern valley wall and the second ~280 m upvalley on the northern valley wall. The lower, southern moraine ridge has ages between 13.6 ± 0.3 and 14.3 ± 0.8 ka (mean 13.9 ± 0.2 ka; peak 13.9 ka), while the higher, northern moraine dates to between 12.4 ± 0.7 and 13.7 ± 1.1 ka (mean 13.0 ± 0.4 ka; peak 13.1 ka) (Fig. 4; Table 2). Ages from the M16 moraine have a normal distribution with a mean age of 13.4 ± 0.3 ka and a peak age of 13.8 ka.

A minor ridge on the valley floor ('M15') has ages that range from 11.6 ± 0.5 to 12.2 ± 0.4 ka (mean 11.9 ± 0.2 ka; peak 12.0 ka). Immediately upvalley of M15, the voluminous moraine complex assigned by van der Hammen et al. (1980) to Drift 5 yields thirteen ages. Nine on the main 'M14' crest range from 10.9 ± 0.3 to 12.4 ± 0.5 ka (mean 11.4 ± 0.5 ka; peak 11.2 ka), and four on the inner 'M13' crest range from 9.8 ± 1.0 to 11.9 ± 0.8 ka (mean 10.9 ± 0.4 ka; peak 11.0 ka) (Fig. 4; Table 2). Two ages from a *roche moutonnée* ~0.5 km inboard of M13 afford a mean age of 11.2 ± 0.6 ka, while two boulders on an adjacent ridge segment give a mean of 1.1 ± 0.1 ka (Fig. 4; Table 2). Finally, three samples from the youngest moraine ('M4') sampled by Jomelli et al. (2014) give a mean age of 0.3 ± 0.2 ka (Fig. 4).

5.3 Paleoglacier and ELA reconstructions

The Pellitero et al. (2015, 2016) approach delivers a range of ELAs that we then compared to the 1955 ELA values (calculated via the same AAR or BR) to derive valley-specific ΔELA values (Table 3). The closest alignment in ΔELA among the three catchments is provided by an AAR of 0.83, which agrees well with modeled and observed AARs (~0.8) for extant tropical glaciers (Kaser and Osmaston, 2002; Stansell et al., 2007). In contrast, ELAs determined using the AABR method were less conclusive with ΔELA values converging at BRs between 19 and 24, considerably higher than previous BR estimates for tropical glaciers that are typically <5 (Lachniet and Vázquez-Salem, 2005; Orvis and Horn, 2000; Quesada-Román et al., 2020; Stansell et al., 2007). We note, however, that ΔELAs determined with AARs of 0.8–0.85 are similar to ELAs calculated with BRs of 5–25. Therefore, recognizing the greater uncertainty in BR suitability, we have chosen to focus on ELAs calculated with an AAR of 0.8.

Whereas ELAs for the Lagunillas and Bocatoma paleo-glacier extents are broadly similar throughout the Lateglacial (Fig. 7), the Ritacuba Negro ELA is consistently higher by ~200 m, potentially reflecting the influence of topography on glacier behavior (see Discussion). For all three glaciers, the magnitude of Lateglacial ΔELAs are dwarfed by the pronounced shifts that followed during the early and late Holocene (Fig. 7). In the Lagunillas valley, the entire span of our glacial record corresponds to a ΔELA of approximately +20 m, reflecting a net warming of as little as ~0.1°C between 13.7 and 11.8 ka (Fig. 7). Nonetheless, the Lagunillas glacier lost ~50% of its full Lateglacial length over that period (Fig. 7), underscoring the important role of glacier configuration in climatic sensitivity (see Discussion).

The neighboring Bocatoma glacier also experienced relatively minor net changes during the Lateglacial period: the difference between the ELA of the Sisuma advance at ~16.6 ka and that of the major subsequent advance culminating at ~12.7 ka is only ~+20 m, corresponding to a warming of ~0.1°C (Fig. 7). The gradual retreat of the terminus between ~12.7 and 11.2 ka reflects a greater ELA rise (+35 m) and stronger warming (0.2°C). The net retreat of the Bocatoma terminus over this period represents 15% of the glacier's full Lateglacial length (Fig. 7). Immediately thereafter, our reconstruction depicts a +120 m rise in ELA during the early Holocene in response to a 0.2°C warming, and a corresponding 25% loss of overall glacier length. Likewise, at the northern end of the range, the net change in ELA on Ritacuba Negro was relatively minor (+77 m) during the Lateglacial, reflecting a warming of <0.5°C, prior to a more pronounced rise in ELA during the early Holocene (Fig. 7).

Since glacier records are rarely continuous, we are unable to resolve the full magnitude of early Holocene ΔELA (and the corresponding ΔT) on the Bocatoma and Ritacuba Negro glaciers, where late Holocene moraines directly overly those older deposits. Episodes of potentially high ELAs that are not documented in our record are represented by dashed lines in Figure 7. In both catchments, however, the absence of middle Holocene deposits is notable, while the magnitude of ΔELA and terminus retreat since deposition of the young (Drift 6) moraines is striking; both glaciers lost >40% of their full Lateglacial length within ~300–500 years (Fig. 7).

By comparing Lateglacial ELA values to the 1955 CE reference ELA value, and using a lapse rate of 6 ± 1°C/km, our results indicate that temperatures at Cocuy were 2–3°C colder than mid-20th Century values during the Lateglacial, and ~1–1.5°C colder during the Drift 6 event, which we correlate broadly to the Little Ice Age.

6. Discussion

The new and recalculated ^{10}Be ages presented here track the behavior of three glacier systems at Cocuy during the Lateglacial period and early Holocene; two datasets (Bocatoma and Ritacuba Negro) extend that record into the Late Holocene. Here, we discuss the overall picture of terminus fluctuations and implications of ΔELAs and climate variability.

Chronology of Lateglacial ice margin fluctuations at Cocuy

In the Lagunillas valley, ages of recessional landforms immediately outside the prominent Pintada and Bocatoma moraines confirm that the glacier occupying this catchment during the LGM had retreated far upvalley by ~16 ka; the glacier had separated into two ice tongues terminating close to their Lateglacial limits (Fig. 2), ~6 km up-valley of the LGM terminus identified by van der Hammen et al. (1980). This timing is significant because it adds to the growing body of glacial-geologic evidence indicating that Heinrich Stadial 1 in the tropics was dominated by widespread deglaciation (Bromley et al., 2009, 2011, 2016; Zech et al., 2007, 2010; Glasser et al., 2009; Jackson et al., 2020), as it was at higher latitudes in both polar hemispheres (Denton et al., 2005, 2022; Foreman et al., 2022, 2025; Hall et al., 2013; Putnam et al., 2013, 2023; Schlücter, 1988; Strand et al., 2022).

Following Heinrich Stadial 1, the Lagunillas and Bocatoma glaciers underwent expansion during the Lateglacial period, when the Pintada and Bocatoma moraines were constructed. We note that this scenario differs slightly from that of van der Hammen et al. (1980), who concluded that the Pintada moraines were significantly older (e.g., Drift 4) than the Bocatoma moraines (Drift 5). That this event was indeed a readvance, as opposed to a pause in retreat, is substantiated by the glacio-tectonized lake sediments incorporated into the Bocatoma terminal moraine (Fig. 6) and by the considerable age offset (2–4 kyr) between the moraine sets and the older deposits immediately distal to them (Fig. 5). Concurrently, advance/stabilization of the Ritacuba Negro glacier resulted in deposition of the M18–M16 moraines in the Cardenillo valley (Jomelli et al., 2014). Whereas earlier studies correlated the Drift 5 deposits with the *El Abra* (Younger Dryas) stadial (e.g., van der Hammen et al., 1980), our ^{10}Be chronology confirms that the advance represented by the Pintada, Bocatoma, and M18–M16 moraines predated the stadial altogether, as proposed by Jomelli et al. (2014, 2017). In the low-gradient Lagunillas and moderate-gradient Cardenillo drainages, the event is represented by multiple moraine ridges deposited between ~14 and 13 ka (Figs. 4, 5). In the high-gradient Bocatoma valley, the composite nature of the terminal moraine likely obscures earlier components of the Lateglacial moraine complex, with deposits from the initial stages of the advance likely being buried under subsequent till layers. Nonetheless, abandonment of this moraine at 12.7 ± 0.4 ka, at the onset of the Younger Dryas stadial, requires that the advance itself occurred prior to this time, in broad accord with the neighboring valleys.

Recognizing that steeper glaciers are likely to be less sensitive to vertical shifts in ELA than glaciers with lower-sloping surfaces (due to the smaller relative impact on accumulation area), it is not surprising that the precipitous Bocatoma ice tongue maintained its full Lateglacial configuration later than did the lower-gradient Lagunillas and Ritacuba Negro glaciers, whose termini responded to subtle positive shifts in ELA (Fig. 7). Nonetheless, the Bocatoma record affords a valuable glaciologic benchmark for the point at which climate warming finally overwhelmed mass balance, driving the Bocatoma glacier into a state of gradual yet determined retreat (Fig. 7). According to our ELA reconstructions, collective retreat of the Cocuy glacial termini represents an atmospheric warming of no more than 0.5°C broadly coincident with the Younger Dryas stadial (Fig. 7).

Implications for Lateglacial climate

The Lateglacial record from Cocuy aligns with a pattern that is consistent across the tropics and described by directly dated moraines sequences, in which mountain glaciers advanced coincident with (though not necessarily due to) the ACR before undergoing net retreat during the subsequent Younger Dryas period. This behavior was reported previously by Stansell et al. (2017) and Jomelli et al. (2014), the latter of whom synthesized Lateglacial moraine records from the northern and southern tropical Andes and highlighted the synchrony among sites spanning a range of latitudes and precipitation regimes. That study invoked a precipitation-cloudiness feedback to explain the pan-equatorial uniformity, speculating that, without such a mechanism, glaciers north of the equator would follow a more 'traditional' Northern Hemisphere Lateglacial climate signal (i.e., retreat during the ACR/Bölling-Alleröd and advance during the Younger Dryas) (Jomelli et al., 2014). Indeed, this model of a north-south contrast in tropical temperature follows the concept of a thermal bipolar seesaw (e.g., Broecker, 1998; Stocker and Johnsen, 2003) and has been explored from both glacial (Rodbell and Seltzer, 2000; Jomelli et al., 2014, 2017; Vázquez-Selem and

Lachniet, 2017; Mey et al., 2020) and palaeoecological (e.g., Stansell et al., 2010; Handiani et al., 2011; Urrego et al., 2016) vantages. We argue, however, that this concept, and thus the mechanism proposed by Jomelli et al. (2014), is unnecessary for two reasons. First, the tropical atmosphere is incapable of sustaining strong horizontal thermal contrasts above the surface layer due to minimal Coriolis forcing, which results in an almost infinite Rossby radius of deformation and the rapid dissipation of anomalies (Hastenrath, 1991; Pierrehumbert, 1995; Sobel et al., 2001; Folkins, 2006; Williams et al., 2009). Recognizing that Termination 1 was characterized by strong latitudinal shifts in precipitation and humidity linked to thermal anomalies at higher latitudes (McGee et al., 2014; Rodbell et al., 2022), it is nonetheless physically implausible for tropical temperature – the main driver of topical mass balance – to have differed measurably across the equator, or indeed throughout the tropics. Second, a growing number of directly dated moraine records from mid and high northern latitudes, including the North Atlantic region (Levy et al., 2016; Wittmeier et al., 2020; Bromley et al., 2023; Putnam et al., 2023), reveal that glaciers there fluctuated broadly in step with those in the tropics and southern mid latitudes (see above) during the Lateglacial, with ACR-age advances and stadial retreat (Sagredo et al., 2018; Denton et al., 2022). From a glacial perspective, at least, the case for antiphased hemispheric temperatures during Termination 1 rests on dubious foundations.

Identifying the mechanism(s) responsible for this pattern of ACR-age glacier growth and stadial retreat in tropical South America is fundamental to establishing the drivers of tropical climate and the causes of abrupt climate changes, both at low latitudes and globally. One potential mechanism is variability in the concentration of atmospheric greenhouse gases, primarily CO_2, which has a clear relationship with Earth's radiative forcing and for which the wind-driven transfer from ocean to atmosphere has been demonstrated (Anderson et al., 2009). At face value, fluctuations in atmospheric CO_2 during the Lateglacial align broadly with the pattern of cryospheric change at Cocuy: periods of glacier retreat coincided with rising atmospheric CO_2 (e.g., the YD), while glacier advance occurred during the CO_2 plateau at ~14.5–12.8 ka (Monnin et al., 2001; Wendt et al., 2024). Further, a CO_2 driver could account for paleo-glaciers at all elevations – from sea level to the high tropical Andes – responding similarly to air temperature as they do today. Upon closer inspection, however, this hypothesis is undermined by the fact that the cryospheric response appears too large relative to any significant change in CO_2-driven radiative forcing. For instance, while the well-documented readvance of glaciers during the ACR reflects a pronounced tropospheric cooling, we note that atmospheric CO_2 concentrations stabilized at that time but did not drop appreciably (Blunier et al., 1997; Monnin et al., 2001; Wendt et al., 2024). Similarly, our Lagunillas and Bocatoma chronologies indicate that both ice tongues had retreated to (and potentially inside of) their respective Lateglacial limits by ~16 ka, as much as two millennia before atmospheric CO_2 attained average Lateglacial concentrations. Together with further discrepancies between the rate and timing of glacier change and atmospheric CO_2 (e.g., Putnam et al., 2013; Bromley et al., 2016; Jackson et al., 2019; Strand et al., 2022), such inconsistencies suggest that CO_2, although a powerful positive feedback (Ganopolski and Kalov, 2011), is unlikely to have shaped Lateglacial tropical climate change.

An alternative driver is tropical ocean-atmospheric heat transfer and the accompanying flux of tropospheric water vapor. Summarizing the potent role of this key greenhouse gas in tropical temperature, Broecker (1997) suggested that changes in water vapor content could account for the high magnitude of tropical cooling observed during glacial periods, while also affording the means for abrupt, hemispherically synchronous climate shifts. The traditional argument against water vapor as a climate driver, however, cites the difficulty in altering the atmospheric vapor budget without first changing temperature, thus consigning water vapor to a positive feedback role. Yet evaporation and latent heating are both fundamental to maintaining the water vapor budget, such that the greenhouse capacity of water vapor and ocean-atmosphere heat transfer are inseparable components of the same system that, together, influence the thermostat of the tropical – and thus global (Pierrehumbert, 1999) – troposphere. This coupling is exemplified today by El Niño-Southern Oscillation (ENSO): perturbations in the coupled latent heating–water vapor flux over the tropical Pacific exert an immediate and global effect on climate (Cane, 1998; Cane and Clement, 1999). A recent hypothesis centered on the Southern Hemisphere ties discrete shifts in mid-latitude atmospheric circulation directly to changes in wind-driven evaporation from the tropical ocean surface (Denton et al., 2021, 2022) and, thus, to the modulation of latent heating and water vapor flux to the overlying troposphere. If true, this coupled mid-latitude–tropical mechanism could induce the pronounced tropical thermal shifts envisaged by Broecker (1997) that would then be propagated globally (Pierrehumbert, 1999). While testing this new hypothesis will require intensive empirical paleoclimate data from all latitudes, we note the strong similarity between tropical glacier-inferred climate records and those from the extra-tropical Southern Hemisphere.

Holocene ice margin fluctuations at Cocuy

Following the Lateglacial, a prominent feature of the Cocuy glacial record is the rapid rise in ELA into the early Holocene, during which both the Bocatoma and Ritacuba Negro glaciers retreated markedly in response to a ~0.75°C warming (Fig. 7). This glaciological event marks a significant climatic shift at 6°N latitude, whereby Andean glaciers transitioned from their Pleistocene configuration to a comparatively contracted Holocene configuration, and appears to be represented elsewhere in the tropics (e.g., Jomelli et al., 2009, 2014; Stansell et al., 2017; Jackson et al., 2020; Doughty et al., 2021). Against this longer-term backdrop, however, the magnitude of ELA rise and glacier retreat in recent centuries clearly dwarfs the glacial oscillations of the last ~14 kyr. The ELA curves for Bocatoma and Ritacuba Negro suggest mean temperatures at Cocuy rose ~1.5°C since culmination of the Little Ice Aage, compared to the fractions-of-a-degree changes that characterized the Lateglacial and early Holocene (Fig. 7). This finding bears a striking resemblance to SST-based calculations of long-term freezing-level height for Cocuy (Ruiz-Carrascal et al., 2022) and reflects glaciologic trends throughout the tropical Andes (Francou et al., 2003; Rabatel et al., 2013; Vuille et al., 2018). A nuanced interpretation of the recent changes requires (1) consensus on the geographic extent and timing of the Little Ice Age and (2) a plausible forcing mechanism for that cooling event. Nonetheless, the profound rise in modern ELA at Cocuy, and the tropical Andes generally, is almost certainly unprecedented in the current interglacial (Gorin et al., 2024), and the coincidence with strongly positive radiative forcing (due to greenhouse gas emissions) is undeniable, fueling the argument that ongoing warming primarily reflects human activity.

7. Conclusions

- Following widespread deglaciation after the LGM, glaciers at Cocuy underwent a pronounced readvance during the Lateglacial period. Cosmogenic ^{10}Be surface-exposure dating of glacial deposits confirm that this advance coincided with the ACR, while the subsequent YD stadial was characterized by gradual yet determined glacier retreat. This cryospheric behavior aligns with a growing number of directly dated moraine records worldwide, suggesting a broadly global pattern of glacier – and, therefore, tropospheric temperature – change during the Lateglacial period. Significantly, this glacial perspective does not support the notion of hemispherically asynchronous temperature fluctuations (i.e., bipolar seesaw) at that time.

- Recognizing that the radiative forcing capacity of CO_2 likely played a role in sustaining mean climate states during the Lateglacial, we propose that CO_2 alone is insufficient as a driver of tropical temperature variability as inferred from the glacier record. Instead, we explore the possibility that abrupt shifts in equatorial ocean-atmosphere heat transfer and vapor flux, potentially linked to mid-latitude atmospheric dynamics, are the primary drivers of Lateglacial temperature variability. As the tropics exert a strong and immediate global influence, any such perturbations of low-latitude climate almost certainly would be transmitted globally.
- The trend of post-ACR deglaciation not only continued into the early Holocene but apparently accelerated, suggesting strong tropospheric warming at Cocuy at that time. At face value, this behavior fits the broader tropical pattern, though we acknowledge that Holocene glacier variability in the tropics is poorly resolved relative to higher latitudes.
- Both the rate and magnitude of deglaciation at Cocuy since the culmination of the LIA are significantly higher than at any other time in our record, and reflect the rapid rise in tropospheric temperature and ELA reported for this site and the tropics generally. This pattern suggests that the scale of modern tropospheric warming is unprecedented within at least the last 16,000 years.

Declaration of competing interest

The authors declare that they have no known competing financial interests or personal relationships that could have appeared to influence the work reported in this paper.

Acknowledgements

Research was funded by the National Science Foundation *Geomorphology and Land Use Dynamics* program (award no. 2022727), the Columbia University Institute for Latin American Studies (ILAS), and Dartmouth College. We thank the Parques Nacionales Naturales de Colombia for permission to access the field area (research permits 006-2018, filing number 20182000049991 and 004-2023, filing number 20232300659691); the Office of the Dean for Research at the Facultad de Minas of the Universidad Nacional de Colombia (UNAL) for allocating funds to support some of the logistics needed for fieldwork activities and for the development of the 1st Course on TCN Applied to Paleoclimate and Paleoglaciology at UNAL-Medellín; Marvin Mosquera Palacios, Isabel Restrepo-Correa, and Ezequiel De Jesùs Ferro-Palacios for fieldwork assistance; local farmers for granting us access to campsites; Peter Croot (University of Galway) for technical assistance; Sonia Eckstein, Evan Barrett, and Alexandra Farnell (Dartmouth College) for laboratory assistance; and Aaron Putnam for constructive discussions and insight. Original ALOS/PALSAR/AVNIR-2 and ALOS-2 ScanSAR data products used in Figures 2, 4, and 5 are provided by JAXA. Prepared in part by LLNL under Contract DE-AC52-07NA27344. This is LLNL-JRNL-2003787.

References

Anderson, R.F., Ali, S., Bradtmiller, L.I., Nielsen, S.H.H., Fleisher, M.Q., Anderson, B.E., Burckle, L.H., 2009. Wind-driven upwelling in the Southern Ocean and the deglacial rise in atmospheric CO_2. *Science* 323, 1443–1448. DOI: 10.1126/science.1167441

Angel, I., Carcaillet, J., Carrillo, E., Beck, C., Audin, L., 2016. Deglaciation chronology in the Mérida Andes from cosmogenic ^{10}Be dating, (Gavidia valley, Venezuela). *Journal of South American Earth Sciences* 71, 235–247. https://doi.org/10.1016/j.jsames.2016.08.001

Bakker, J., 1990. *Tectonic and Climatic Controls on Late Quaternary Sedimentary Processes in a Neotectonic Intramontane Basin, the Pitalito Basin, South Colombia* (Ph.D.). Wageningen University and Research, Netherlands. Retrieved from https://www.proquest.com/docview/2568201634/abstract/8409E656EA684573PQ/1

Balco, G., 2011. Contributions and unrealized potential contributions of cosmogenic-nuclide exposure dating to glacier chronology, 1990–2010. *Quaternary Science Reviews* 30, 3–27. https://doi.org/10.1016/j.quascirev.2010.11.003

Balco, G., 2020. Glacier Change and Paleoclimate Applications of Cosmogenic-Nuclide Exposure Dating. *Annual Review of Earth and Planetary Sciences* 48, 21–48. https://doi.org/10.1146/annurev-earth-081619-052609

Barr, I.D., Lovell, H., 2014. A review of topographic controls on moraine distribution. *Geomorphology* 226, 44–64. https://doi.org/10.1016/j.geomorph.2014.07.030

Barry, R.G., Chorley, R.J., 2003. Atmosphere, weather and climate, 8th edition (1st edition 1968). Routledge, London, p. 25

Benn, D.I., Evans, D.J.A., 1998. Glaciers and Glaciation, first edition. Edward Arnold, London. 734 pp.

Benn, D.I., Hulton, N.R.J., 2010. An Excel™ spreadsheet program for reconstructing the surface profile of former mountain glaciers and ice caps. *Computers & Geosciences* 36, 605–610. https://doi.org/10.1016/j.cageo.2009.09.016

Benn, D.I., Lehmkuhl, F., 2000. Mass balance and equilibrium-line altitudes of glaciers in high-mountain environments. *Quaternary International* 65–66, 15–29. https://doi.org/10.1016/S1040-6182(99)00034-8

Benn, D.I., Owen, L.A., Osmaston, H.A., Seltzer, G.O., Porter, S.C., Mark, B., 2005. Reconstruction of equilibrium-line altitudes for tropical and sub-tropical glaciers. *Quaternary International* 138–139, 8–21. https://doi.org/10.1016/j.quaint.2005.02.003

Blard, P.-H., Braucher, R., Lavé, J., Bourlès, D., 2013. Cosmogenic 10Be production rate calibrated against 3He in the high Tropical Andes (3800–4900 m, 20–22° S). *Earth and Planetary Science Letters* 382, 140–149. https://doi.org/10.1016/j.epsl.2013.09.010

Blunier, T., Schwander, J., Stauffer, B., Stocker, T., Dällenbach, A., Indermühle, A., Tschumi, J., Chappellaz, J., Raynaud, D., Barnola, J.M., 1997. Timing of the Antarctic Cold Reversal and the atmospheric CO2 increase with respect to the Younger Dryas event. *Geophysical Research Letters* 24, 2683–2686. https://doi.org/10.1029/97GL02658

Bradley, R.S., Vuille, M., Hardy, D., Thompson, L.G., 2003. Low latitude ice cores record Pacific sea surface temperatures. *Geophysical Research Letters* 30. https://doi.org/10.1029/2002GL016546

Broecker, W.S., 1997. Mountain glaciers: Recorders of atmospheric water vapor content?. *Global Biogeochemical Cycles* 11, 589–597. https://doi.org/10.1029/97GB02267

Broecker, W.S., 1998. Paleocean circulation during the last deglaciation: A bipolar seesaw? *Paleoceanography* 13, 119–121.

Bromley, G.R., Schaefer, J.M., Winckler, G., Hall, B.L., Todd, C.E., Rademaker, K.M., 2009. Relative timing of last glacial maximum and late-glacial events in the central tropical Andes. *Quaternary Science Reviews* 28, 2514–2526. https://doi.org/10.1016/j.quascirev.2009.05.012

Bromley, G.R., Hall, B.L., Schaefer, J.M., Winckler, G., Todd, C.E., Rademaker, K.M., 2011. Glacier fluctuations in the southern Peruvian Andes during the late-glacial period, constrained with cosmogenic ^{3}He. *Journal of Quaternary Science* 26, 37–43. https://doi.org/10.1002/jqs.142

Bromley, G.R.M., Schaefer, J.M., Hall, B.L., Rademaker, K.M., Putnam, A.E., Todd, C.E., et al., 2016. A cosmogenic ^{10}Be chronology for the local last glacial maximum and termination in the Cordillera Oriental, southern Peruvian Andes: Implications for the tropical role in global climate. *Quaternary Science Reviews* 148, 54–67. https://doi.org/10.1016/j.quascirev.2016.07.010

Bromley, G., Putnam, A., Hall, B., Rademaker, K., Thomas, H., Balter-Kennedy, A., Barker, S., Rice, D., 2023. Lateglacial shifts in seasonality reconcile conflicting North Atlantic temperature signals. *Journal of Geophysical Research: Earth Surface* 128, p.e2022JF00695. https://doi.org/10.1029/2022JF006951

Cane, M.A., 1998. A role for the tropical Pacific. *Science* 282, 59–61. DOI: 10.1126/science.282.5386.59

Cane, M., Clement, A.C., 1999. A role for the tropical Pacific coupled ocean-atmosphere system on Milankovitch and millennial timescales part II: Global impacts. *Geophysical Monograph-American Geophysical Union* 112, 373–384.

Carcaillet, J., Angel, I., Carrillo, E., Audemard, F.A., Beck, C., 2013. Timing of the last Deglaciation in the Sierra Nevada of the Mérida Andes, Venezuela. *Quaternary Research* 80, 482–494. https://doi.org/10.1016/j.yqres.2013.08.001

Chiang, J.C.H., 2009. The tropics in paleoclimate. *Annual Review of Earth and Planetary Sciences* 37, 263–297.

DeForest Safford, H., 1999. Brazilian Páramos I. An introduction to the physical environment and vegetation of the campos de altitude. *Journal of Biogeography* 26, 693–712. https://doi.org/10.1046/j.1365-2699.1999.00313.x

Denton, G.H., Alley, R.B., Comer, G.C., Broecker, W.S., 2005. The role of seasonality in abrupt climate change. *Quaternary Science Reviews* 24, 1159–1182. https://doi.org/10.1016/j.quascirev.2004.12.002

Denton, G.H., Putnam, A.E., Russell, J.L., Barrell, D.J.A., Schaefer, J.M., Kaplan, M.R., Strand, P.D., 2021. The Zealandia Switch: Ice age climate shifts viewed from Southern Hemisphere moraines. *Quaternary Science Reviews* 257, 106771. https://doi.org/10.1016/j.quascirev.2020.106771

Denton, G.H., Toucanne, S., Putnam, A.E., Barrell, D.J., Russell, J.L., 2022. Heinrich summers. *Quaternary Science Reviews* 295, 107750. https://doi.org/10.1016/j.quascirev.2022.107750

Doughty, A.M., Kelly, M.A., Russell, J.M., Jackson, M.S., Anderson, B.A., Chipman, J., Nakileza, B., Dee, S.G., 2020, Modeling glacier extents and equilibrium line altitudes in the Rwenzori Mountains, Uganda, over the last 31,000 yr, in Waitt, R.B., Thackray, G.D., and Gillespie, A.R., eds., Untangling the Quaternary Period: A Legacy of Stephen C. Porter: Geological Society of America Special Paper 548, p. 171–188, https://doi.org/10.1130/2020.2548(09)

Fabre, A., Osorio, M., Vargas, R., 1984. Geología de la Plancha 153 Chita. Bogotá. INGEOMINAS.

Farrera, I., Harrison, S.P., Prentice, I.C., Ramstein, G., Guiot, J., Bartlein, P.J., et al., 1999. Tropical climates at the Last Glacial Maximum: a new synthesis of terrestrial palaeoclimate data. I. Vegetation, lake-levels, and geochemistry. *Climate Dynamics* 15, 823–856. https://doi.org/10.1007/s003820050317

Favier, V., Wagnon, P., Chazarin, J.-P., Maisincho, L., Coudrain, A., 2004. One-year measurements of surface heat budget on the ablation zone of Antizana Glacier 15, Ecuadorian Andes. *Journal of Geophysical Research: Atmospheres* 109(D18). https://doi.org/10.1029/2003JD004359

Folkins, I., 2006. Convective damping of buoyancy anomalies and its effect on lapse rates in the tropical lower troposphere. *Atmospheric Chemistry and Physics* 6, 1–12. https://doi.org/10.5194/acp-6-1-2006

Foreman, A.C., Bromley, G.R.M., Hall, B.L., Jackson, M.S., 2022. A ^{10}Be-dated record of glacial retreat in Connemara, Ireland, following the last glacial maximum and implications for regional climate. *Palaeogeography, Palaeoclimatology, Palaeoecology* 592, p.110901. https://doi.org/10.1016/j.palaeo.2022.110901

Foreman, A.C., Bromley, G.R., Hall, B.L., Rodríguez, P.C., 2025. Thinning and retreat of the temperate Connemara ice centre, Ireland, during Heinrich Stadial 1 constrained with cosmogenic ^{10}Be dating. *Geomorphology* 475, p.109661. https://doi.org/10.1016/j.geomorph.2025.109661

Francou, B., Vuille, M., Wagnon, P., Mendoza, J., Sicart, J.-E., 2003. Tropical climate change recorded by a glacier in the central Andes during the last decades of the Twentieth Century: Chacaltaya, Bolivia, 16°S. *Journal of Geophysical Research: Atmospheres* 108(D5). https://doi.org/10.1029/2002JD002959

Ganopolski, A., Calov, R., 2011. The role of orbital forcing, carbon dioxide and regolith in 100 kyr glacial cycles. *Climate of the Past* 7, 1415–1425. https://doi.org/10.5194/cp-7-1415-2011

Garelick, S., Russell, J., Richards, A., Smith, J., Kelly, M., Anderson, N., Jackson, M.S., Doughty, A., Nakileza, B., Ivory, S., Dee, S., 2022. The dynamics of warming during the last deglaciation in high-elevation regions of Eastern Equatorial Africa. *Quaternary Science Reviews* 281, 107416. https://doi.org/10.1016/j.quascirev.2022.107416

Glasser, N.F., Clemmens, S., Schnabel, C., Fenton, C.R., McHargue, L., 2009. Tropical glacier fluctuations in the Cordillera Blanca, Peru between 12.5 and 7.6 ka from cosmogenic 10Be dating. *Quaternary Science Reviews* 28, 3448–3458. https://doi.org/10.1016/j.quascirev.2009.10.006

Gonzalez, E., van der Hammen, T., Foster Flint, R., 1965. Late Quaternary glacial and vegetational sequence in Valle de Lagunillas, Sierra Nevada del Cocuy, Colombia. *Leidse Geologische Mededelingen* 323, 157–182.

Gorin, A.L., Shakun, J.D., Jones, A.G., Kennedy, T.M., Marcott, S.A., Goehring, B.M., Zoet, L.K., Jomelli, V., Bromley, G.R., Mateo, E.I., Mark, B.G., 2024. Recent tropical Andean glacier retreat is unprecedented in the Holocene. *Science* 385, 517–521. DOI: 10.1126/science.adg7546

Hall, B.L., Porter, C.T., Denton, G.H., Lowell, T.V., Bromley, G.R., 2013. Extensive recession of Cordillera Darwin glaciers in southernmost South America during Heinrich stadial 1. *Quaternary Science Reviews* 62, 49–55. https://doi.org/10.1016/j.quascirev.2012.11.026

Handiani, D., Paul, A., Dupont, L., 2011. Tropical climate and vegetation changes during Heinrich Event 1: comparing climate model output to pollen-based vegetation reconstructions with emphasis on the region around the tropical Atlantic Ocean. *Climate of the Past Discussions* 7.

Hastenrath, S., 1991. Climate Dynamics of the Tropics. Springer, p. 488. https://doi.org/10.1007/978-94-011-3156-8

Hastenrath, S., 2009. Past glaciation in the tropics. *Quaternary Science Reviews* 28, 790–798. https://doi.org/10.1016/j.quascirev.2008.12.004

Helmens, K.F., Rutter, N.W., Kuhry, P., 1997. Glacier fluctuations in the Eastern Andes of Colombia (south America) during the last 45,000 radiocarbon years. *Quaternary International* 38–39, 39–48. https://doi.org/10.1016/S1040-6182(96)00021-3

Jackson, M.S., Kelly, M.A., Russell, J.M., Doughty, A.M., Howley, J.A., Chipman, J.W., et al., 2019. High-latitude warming initiated the onset of the last deglaciation in the tropics. *Science Advances* 5, eaaw2610. https://doi.org/10.1126/sciadv.aaw2610

Jackson, M.S., Kelly, M.A., Russell, J.M., Doughty, A.M., Howley, J.A., Chipman, J.W., et al., 2020. Glacial fluctuations in tropical Africa during the last glacial termination and implications for tropical climate following the Last Glacial Maximum. *Quaternary Science Reviews* 243, 106455. https://doi.org/10.1016/j.quascirev.2020.106455

Jomelli, V., Favier, V., Rabatel, A., Brunstein, D., Hoffmann, G., Francou, B., 2009. Fluctuations of glaciers in the tropical Andes over the last millennium and palaeoclimatic implications: A review. *Palaeogeography, Palaeoclimatology, Palaeoecology* 281, 269–282.

Jomelli, V., Favier, V., Vuille, M., Braucher, R., Martin, L., Blard, P.-H., et al., 2014. A major advance of tropical Andean glaciers during the Antarctic cold reversal. *Nature* 513, 224–228. https://doi.org/10.1038/nature13546

Jomelli, V., Martin, L., Blard, P. H., Favier, V., Vuillé, M., Ceballos, J.L., 2017. Revisiting the Andean tropical glacier behavior during the Antarctic cold reversal. *Cuadernos de Investigación Geográfica* 43, 629–648. https://doi.org/10.18172/cig.3201

Kammer, A., Piraquive, A., Gómez, C., Mora, A., Velásquez, A., Gómez, J., Mateus-Zabala, D., 2020. Structural styles of the Eastern Cordillera of Colombia. *The geology of Colombia* 3, 143–183. https://doi.org/10.32685/pub.esp.37.2019.06

Kaser, G., Osmaston, H., 2002. *Tropical Glaciers*. Cambridge University Press.

Kelly, M.A., Lowell, T.V., Applegate, P.J., Phillips, F.M., Schaefer, J.M., Smith, C.A., et al. 2015. A locally calibrated, late glacial ^{10}Be production rate from a low-latitude, high-altitude site in the Peruvian Andes. *Quaternary Geochronology* 26, 70–85. https://doi.org/10.1016/j.quageo.2013.10.007

Kuhry, P., Hooghiemstra, H., van Geel, B., van der Hammen, T., 1993. The El Abra stadial in the Eastern Cordillera of Colombia (South America). *Quaternary Science Reviews* 12, 333–343. https://doi.org/10.1016/0277-3791(93)90041-J

Lachniet, M.S., Vazquez-Selem, L., 2005. Last Glacial Maximum equilibrium line altitudes in the circum-Caribbean (Mexico, Guatemala, Costa Rica, Colombia, and Venezuela). *Quaternary International* 138–139, 129–144. https://doi.org/10.1016/j.quaint.2005.02.010

Lal, D., 1991. Cosmic ray labeling of erosion surfaces: in situ nuclide production rates and erosion models. *Earth and Planetary Science Letters* 104, 424–439. https://doi.org/10.1016/0012-821X(91)90220-C

Legrain, E., Blard, P.H., Kageyama, M., Charreau, J., Leduc, G., Bourdin, S., Bekaert, D.V., 2023. Moisture amplification of the high-altitude deglacial warming. *Quaternary Science Reviews* 318, 108303. https://doi.org/10.1016/j.quascirev.2023.108303

Levy, L.B., Kelly, M.A., Lowell, T.V., Hall, B.L., Howley, J.A., Smith, C.A., 2016. Coeval fluctuations of the Greenland ice sheet and a local glacier, central East Greenland, during late glacial and early Holocene time. *Geophysical Research Letters* 43, 1623–1631. https://doi.org/10.1002/2015GL067108

Lifton, N., Caffee, M., Finkel, R., Marrero, S., Nishiizumi, K., Phillips, F. M., et al., 2015. In situ cosmogenic nuclide production rate calibration for the CRONUS-Earth project from Lake Bonneville, Utah, shoreline features. *Quaternary Geochronology* 26, 56–69. https://doi.org/10.1016/j.quageo.2014.11.002

Loomis, S.E., Russell, J.M., Verschuren, D., Morrill, C., De Cort, G., Sinninghe Damsté, J. S., et al., 2017. The tropical lapse rate steepened during the Last Glacial Maximum. *Science Advances* 3, e1600815. https://doi.org/10.1126/sciadv.1600815

López-Moreno, J.I., Rojas-Heredia, F., Ceballos, J.L., Morán-Tejeda, E., Alonso-González, E., Vidaller, I., et al., 2022. Recent evolution of glaciers in the Cocuy-Güicán Mountains (Colombian Andes) and the hydrological implications. *Land Degradation & Development* ldr.4336. https://doi.org/10.1002/ldr.4336

Mackintosh, A.N., Anderson, B.M., Pierrehumbert, R.T., 2017. Reconstructing climate from glaciers. *Annual Review of Earth and Planetary Sciences* 45, 649–680. https://doi.org/10.1146/annurev-earth-063016-020643

Mahaney, W.C., Milner, M.W., Kalm, V., Dirszowsky, R.W., Hancock, R.G.V., Beukens, R.P., 2008. Evidence for a Younger Dryas glacial advance in the Andes of northwestern Venezuela. *Geomorphology* 96, 199–211. https://doi.org/10.1016/j.geomorph.2007.08.002

Martin, L.C.P., Blard, P.-H., Lavé, J., Braucher, R., Lupker, M., Condom, T., et al., 2015. In situ cosmogenic ^{10}Be production rate in the high tropical Andes. *Quaternary Geochronology* 30, 54–68. https://doi.org/10.1016/j.quageo.2015.06.012

Martin, L.C.P., Blard, P.-H., Lavé, J., Jomelli, V., Charreau, J., Condom, T., et al. (2020). Antarctic-like temperature variations in the tropical Andes recorded by glaciers and lakes during the last deglaciation. *Quaternary Science Reviews* 247, 106542. https://doi.org/10.1016/j.quascirev.2020.106542

Masiokas, M.H., Rabatel, A., Rivera, A., Ruiz, L., Pitte, P., Ceballos, J. L., et al., 2020. A review of the current state and recent changes of the Andean cryosphere. *Frontiers in Earth Science* 8, Retrieved from https://www.frontiersin.org/article/10.3389/feart.2020.00099

McGee, D., Donohoe, A., Marshall, J., Ferreira, D., 2014. Changes in ITCZ location and cross-equatorial heat transport at the Last Glacial Maximum, Heinrich Stadial 1, and the mid-Holocene. *Earth and Planetary Science Letters* 390, 69–79.

Mendivelso, D., 2016. The El Cocuy snowy range. In M. Hermelin (Ed.), *Landscapes and Landforms of Colombia* (pp. 85–98). Cham: Springer International Publishing. https://doi.org/10.1007/978-3-319-11800-0_7

Mey, J., D'Arcy, M.K., Schildgen, T.F., Egholm, D.L., Wittmann, H., Strecker, M.R., 2020. Temperature and precipitation in the southern Central Andes during the last glacial maximum, Heinrich Stadial 1, and the Younger Dryas. *Quaternary Science Reviews* 248, 106592.

Molano, S.M., Cardenas, D.P., Snaider Gómez, H., Alvarado, D.M., Galindo, A.F., Sanabria, J.F., Gómez-Neita, J.S., 2022. Evaluación del retroceso glaciar de la Sierra Nevada del Cocuy, Colombia a partir de la clasificación de imágenes multisensor. *Boletín de Geología* 44, 49–73. https://doi.org/10.18273/revbol.v44n1-2022002

Monnin, E., Indermühle, A., Dällenbach, A., Flückiger, J., Stauffer, B., Stocker, T.F., Raynaud, D., Barnola, J.M., 2001. Atmospheric CO2 concentrations over the last glacial termination. *Science* 29, 112–114. DOI: 10.1126/science.291.5501.112

Nishiizumi, K., Winterer, E.L., Kohl, C.P., Klein, J., Middleton, R., Lal, D., Arnold, J.R., 1989. Cosmic ray production rates of ^{10}Be and ^{26}Al in quartz from glacially polished rocks. *Journal of Geophysical Research: Solid Earth* 94, 17907–17915. https://doi.org/10.1029/JB094iB12p17907

Oerlemans, J., 1989. On the response of valley glaciers to climatic change. In Johannes Oerlemans (Ed.), *Glacier Fluctuations and Climatic Change* (pp. 353–371). Dordrecht: Springer Netherlands. https://doi.org/10.1007/978-94-015-7823-3_23

Orvis, K.H., Horn, S.P., 2000. Quaternary glaciers and climate on Cerro Chirripó, Costa Rica. *Quaternary Research* 54, 24–37. https://doi.org/10.1006/qres.2000.2142

Pellitero, R., Rea, B.R., Spagnolo, M., Bakke, J., Hughes, P., Ivy-Ochs, S., et al., 2015. A GIS tool for automatic calculation of glacier equilibrium-line altitudes. *Computers & Geosciences* 82, 55–62. https://doi.org/10.1016/j.cageo.2015.05.005

Pellitero, R., Rea, B.R., Spagnolo, M., Bakke, J., Ivy-Ochs, S., Frew, C.R., et al., 2016. GlaRe, a GIS tool to reconstruct the 3D surface of palaeoglaciers. *Computers & Geosciences* 94, 77–85. https://doi.org/10.1016/j.cageo.2016.06.008

Pierrehumbert, R.T., 1995. Thermostat, radiator fins, and local runaway greenhouse. *Journal of Atmospheric Science* 52, 1784–1806.

Pierrehumbert, R.T., 1999. Subtropical water vapor as a mediator of rapid global climate change. *Geophysical Monograph-American Geophysical Union* 112, 339–362.

Porter, S.C., 2000. Snowline depression in the tropics during the Last Glaciation. *Quaternary Science Reviews* 20, 1067–1091. https://doi.org/10.1016/S0277-3791(00)00178-5

Putnam, A.E., Schaefer, J.M., Denton, G.H., Barrell, D.J., Andersen, B.G., Koffman, T.N., Rowan, A.V., Finkel, R.C., Rood, D.H., Schwartz, R., Vandergoes, M.J., 2013. Warming and glacier recession in the Rakaia valley, Southern Alps of New Zealand, during Heinrich Stadial 1. *Earth and Planetary Science Letters* 382, 98–110. https://doi.org/10.1016/j.epsl.2013.09.005

Putnam, A.E., Denton, G.H., Schaefer, J.M., 2023. A ^{10}Be chronology of the Esmark Moraine and Lysefjorden region, southwestern Norway: Evidence for coeval glacier resurgence in both polar hemispheres during the Antarctic Cold Reversal. *Quaternary Science Reviews* 316, p.108259. https://doi.org/10.1016/j.quascirev.2023.108259

Quesada-Román, A., Campos, N., Alcalá-Reygosa, J., Granados-Bolaños, S., 2020. Equilibrium-line altitude and temperature reconstructions during the Last Glacial Maximum in Chirripó National Park, Costa Rica. *Journal of South American Earth Sciences* 100, 102576. https://doi.org/10.1016/j.jsames.2020.102576

Rabatel, A., Francou, B., Soruco, A., Gomez, J., Cáceres, B., Ceballos, J.L., et al., 2013. Current state of glaciers in the tropical Andes: a multi-century perspective on glacier evolution and climate change. *The Cryosphere* 7, 81–102. https://doi.org/10.5194/tc-7-81-2013

Rabatel, A., Ceballos, J.L., Micheletti, N., Jordan, E., Braitmeier, M., González, J., et al., 2017. Toward an imminent extinction of Colombian glaciers? *Geografiska Annaler: Series A, Physical Geography* 100, 75–95. https://doi.org/10.1080/04353676.2017.1383015

Rea, B.R., 2009. Defining modern day Area-Altitude Balance Ratios (AABRs) and their use in glacier-climate reconstructions. *Quaternary Science Reviews* 28, 237–248. https://doi.org/10.1016/j.quascirev.2008.10.011

Reimer, P.J., Austin, W.E.N., Bard, E., Bayliss, A., Blackwell, P.G., Ramsey, C.B., et al., 2020. The IntCal20 Northern Hemisphere radiocarbon age calibration curve (0–55 cal kBP). *Radiocarbon* 62, 725–757. https://doi.org/10.1017/RDC.2020.41

Restrepo-Moreno, S.A., Foster, D.A., Bernet, M., Min, K., Noriega, S., 2019. Morphotectonic and orogenic development of the Northern Andes of Colombia: A low-temperature thermochronology perspective. *Geology and Tectonics of Northwestern South America: The Pacific-Caribbean-Andean Junction*, pp.749–832. https://doi.org/10.1007/978-3-319-76132-9_11

Rodbell, D.T., Seltzer, G.O., 2000. Rapid ice margin fluctuations during the Younger Dryas in the tropical Andes. *Quaternary Research* 54, 328–338. https://doi.org/10.1006/qres.2000.2177

Rodbell, D.T., Smith, J.A., Mark, B.G., 2009. Glaciation in the Andes during the Lateglacial and Holocene. *Quaternary Science Reviews* 28, 2165–2212. https://doi.org/10.1016/j.quascirev.2009.03.012

Rodbell, D.T., Hatfield, R.G., Abbott, M.B., Chen, C.Y., Woods, A., Stoner, J.S., McGee, D., Tapia, P.M., Bush, M., Valero-Garcés, B.L., Lehmann, S.B., 2022. 700,000 years of tropical Andean glaciation. *Nature* 607, 301–306. https://doi.org/10.1038/s41586-022-04873-0

Ruiz-Carrascal, D., González-Duque, D., Restrepo-Correa, I., 2022. Two-tiered reconstruction of Late Pleistocene to Holocene changes in the freezing level height in the largest glacierized areas of the Colombian Andes. *Journal of Mountain Science* 19, 615–636. https://doi.org/10.1007/s11629-021-6783-6

Rupper, S., Roe, G., 2008. Glacier changes and regional climate: A mass and energy balance approach. *Journal of Climate* 21, 5384–5401. https://doi.org/10.1175/2008JCLI2219.1

Sagredo, Esteban A., Rupper, S., Lowell, T.V., 2014. Sensitivities of the equilibrium line altitude to temperature and precipitation changes along the Andes. *Quaternary Research* 81, 355–366. https://doi.org/10.1016/j.yqres.2014.01.008

Sagredo, E.A., Kaplan, M.R., Araya, P.S., Lowell, T.V., Aravena, J.C., Moreno, P.I., Kelly, M.A. Schaefer, J.M., 2018. Trans-pacific glacial response to the Antarctic Cold Reversal in the southern mid-latitudes. *Quaternary Science Reviews* 188, 160–166. https://doi.org/10.1016/j.quascirev.2018.01.011

Schaefer, J.M., Denton, G.H., Kaplan, M., Putnam, A., Finkel, R.C., Barrell, D.J.A., et al., 2009. High-frequency Holocene glacier fluctuations in New Zealand differ from the northern signature. *Science* 324, 622–625. https://doi.org/10.1126/science.1169312

Schlüchter, C., 1988. The deglaciation of the Swiss-Alps: a paleoclimatic event with chronological problems. *Quaternaire* 25, 141–145.

Seager, R., Battisti, D.S., 2007. Challenges to our understanding of the general circulation: Abrupt climate change. *Global circulation of the atmosphere* 331, p.371. https://doi.org/10.1515/9780691236919-014

Shakun, J.D., Clark, P.U., Marcott, S.A., Brook, E.J., Lifton, N.A., Caffee, M., Shakun, W.R., 2015. Cosmogenic dating of Late Pleistocene glaciation, southern tropical Andes, Peru. *Journal of Quaternary Science* 30, 841–847. https://doi.org/10.1002/jqs.2822

Smith, J.A., Seltzer, G.O., Farber, D.L., Rodbell, D.T., Finkel, R.C., 2005. Early local last glacial maximum in the tropical Andes. *Science* 308, 678–681. https://doi.org/10.1126/science.1107075

Sobel, A.H., Nilsson, J. and Polvani, L.M., 2001. The weak temperature gradient approximation and balanced tropical moisture waves. *Journal of the Atmospheric Sciences* 58, 3650–3665. https://doi.org/10.1175/1520-0469(2001)058<3650:TWTGAA>2.0.CO;2

Stansell, N.D., Polissar, P.J., Abbott, M.B., 2007. Last glacial maximum equilibrium-line altitude and paleo-temperature reconstructions for the Cordillera de Mérida, Venezuelan Andes. *Quaternary Research* 67, 115–127. https://doi.org/10.1016/j.yqres.2006.07.005

Stansell, N.D., Abbott, M.B., Rull, V., Rodbell, D.T., Bezada, M., Montoya, E., 2010. Abrupt Younger Dryas cooling in the northern tropics recorded in lake sediments from the Venezuelan Andes. *Earth and Planetary Science Letters* 293, 154–163. https://doi.org/10.1016/j.epsl.2010.02.040

Stansell, N.D., Licciardi, J.M., Rodbell, D.T., Mark, B.G., 2017. Tropical ocean-atmospheric forcing of Late Glacial and Holocene glacier fluctuations in the Cordillera Blanca, Peru. *Geophysical Research Letters* 44, 4176–4185. https://doi.org/10.1002/2016GL072408

Stocker, T.F., Johnsen, S.J., 2003. A minimum thermodynamic model for the bipolar seesaw. *Paleoceanography* 18. https://doi.org/10.1029/2003PA000920

Stone, J.O., 2000. Air pressure and cosmogenic isotope production. *Journal of Geophysical Research: Solid Earth* 105, 23753–23759. https://doi.org/10.1029/2000JB900181

Strand, P.D., Putnam, A.E., Sambuu, O., Putnam, D.E., Denton, G.H., Schaefer, J.M., Radue, M.J., Dorj, A., Amarsaikhan, P., Stevens, J., Cole, D.G., 2022. A ^{10}Be moraine chronology of the last glaciation and termination at 49 N in the Mongolian Altai of Central Asia. *Paleoceanography and Paleoclimatology* 37, p.e2022PA004423. https://doi.org/10.1029/2022PA004423

Sturm, H., Rangel Churío, J., 1985. *Ecología de los páramos andinos : una visión preliminar integrada.* Universidad Nacional de Colombia. Instituto de Ciencias Naturales. Museo de Historia Natural.

Taylor, R.G., Mileham, L., Tindimugaya, C., Majugu, A., Muwanga, A., Nakileza, B., 2006. Recent glacial recession in the Rwenzori Mountains of East Africa due to rising air temperature. *Geophysical Research Letters* 33. https://doi.org/10.1029/2006GL025962

Urrego, D.H., Hooghiemstra, H., Rama-Corredor, O., Martrat, B., Grimalt, J.O., Thompson, L., Bush, M.B., González-Carranza, Z., Hanselman, J., Valencia, B., Velásquez-Ruiz, C., 2016. Millennial-scale vegetation changes in the tropical Andes using ecological grouping and ordination methods. *Climate of the Past* 12, 697–711. https://doi.org/10.5194/cp-12-697-2016

van der Hammen, T., Gonzalez, E., 1960. Upper Pleistocene and Holocene climate and vegetation of the "Sabana de Bogota" (Colombia, South America). *Leidse Geologische Mededelingen* 25, 261–315.

van der Hammen, T., Barelds, J., De Jong, H., De Veer, A.A., 1980. Glacial sequence and environmental history in the Sierra Nevada del Cocuy (Colombia). *Palaeogeography, Palaeoclimatology, Palaeoecology* 32, 247–340. https://doi.org/10.1016/0031-0182(80)90043-7 van der Hammen, T., Hooghiemstra, H., 1995. The El Abra stadial, a Younger Dryas equivalent in Colombia. *Quaternary Science Reviews* 14, 841–851. https://doi.org/10.1016/0277-3791(95)00066-6

Vázquez-Selem, L. and Lachniet, M.S., 2017. The deglaciation of the mountains of Mexico and Central America. *Cuadernos de investigación geográfica: Geographical Research Letters* 43, 553–570.

Vuille, M., Carey, M., Huggel, C., Buytaert, W., Rabatel, A., Jacobsen, D., Soruco, A., Villacis, M., Yarleque, C., Timm, O.E., Condom, T., 2018. Rapid decline of snow and ice in the tropical Andes–Impacts, uncertainties, and challenges ahead. *Earth-science reviews* 176, 195–213.

Wendt, K., 2024. CO_2 amount fractions from WAIS Divide, Antarctica. U.S. Antarctic Program (USAP) Data Center. https://doi.org/10.15784/601775.

Williams, I.N., Pierrehumbert, R.T., Huber, M., 2009. Global warming, convective threshold and false thermostats. *Geophysical Research Letters* 36. https://doi.org/10.1029/2009GL039849

Wittmeier, H.E., Schaefer, J.M., Bakke, J., Rupper, S., Paasche, Ø., Schwartz, R., Finkel, R.C., 2020. Late Glacial mountain glacier culmination in Arctic Norway prior to the Younger Dryas. *Quaternary Science Reviews* 245, p.106461. https://doi.org/10.1016/j.quascirev.2020.106461

Zech, R., Kull, C., Kubik, P.W., Veit, H., 2007. LGM and Late Glacial glacier advances in the Cordillera Real and Cochabamba (Bolivia) deduced from ^{10}Be surface exposure dating. *Climate of the Past* 3, 623–635. https://doi.org/10.5194/cp-3-623-2007

Zech, J., Zech, R., May, J.-H., Kubik, P.W., Veit, H., 2010. Lateglacial and early Holocene glaciation in the tropical Andes caused by La Niña-like conditions. *Palaeogeography, Palaeoclimatology, Palaeoecology* 293, 248–254. https://doi.org/10.1016/j.palaeo.2010.05.026

FIGURE CAPTIONS

Fig. 1. (A) Topographic map of South America indicating the position of panel B (white rectangle) and the Sierra Nevada del Cocuy; **(B)** Mean annual precipitation map for Colombia (1979–2018) derived from the Climate Reanalyzer (https://ClimateReanalyzer.org), showing the location of the Sierra Nevada del Cocuy in the Cordillera Oriental. **(C)** Topographic map of the Sierra Nevada del Cocuy, indicating our Lagunillas study area in the southern range and the Cardenillo valley on Ritacuba Negro in the northern part, along with the locations of sites mentioned in the text.

Principal summits of the range are 1) Pan de Azúcar, 2) Cóncavo, 3) San Pablín Sur, 4) San Pablín Norte, 5) Ritacuba Blanco, 6) Ritacuba Negro, and 7) Ritacuba Norte.

Fig. 2. Glacial geomorphology of the upper Lagunillas and Bocatoma catchments, illustrating the distribution of deposits and key moraine units discussed in the text.

Fig. 3. (A) The southern half of the Lagunillas valley viewed from the north, showing the location of sedimentary exposure VL-V reported by Gonzalez et al. (1965). Visible just beyond VL-V are the prominent Bocatoma lateral moraines entering the Lagunillas valley from the left. **(B)** Terminal moraines in the upper Lagunillas valley, with moraine-dammed Laguna La Parada in the middle distance and sample locations identified. **(C)** Bocatoma lateral-terminal moraine complex viewed from the Sisuma moraine crest, with sample locations identified. **(D)** Drift 6 (Little Ice Age) deposits overlying older glacial drift in the upper Bocatoma valley.

Fig. 4. Glacial geomorphology of the Cardenillo valley on Ritacuba Negro, depicting the distribution of deposits as reported by Jomelli et al. (2014), along with ^{10}Be surface-exposure ages recalculated as described in section 4.2. (Right) Specific landform age statistics represented by normal kernel density plots, in which ages of individual samples are shown as thin black lines and cumulative age distributions as thick black lines. Mean age and 1σ uncertainty are represented by the vertical blue lines and yellow shading, respectively. Samples rejected as outliers are depicted by dashed lines.

Fig. 5. Glacial geomorphology and ^{10}Be chronology for the Lagunillas and Bocatoma catchments, including landform-specific age statistics for key depositional units. For geomorphic legend, see Figure 2. Surface-exposure ages correspond to values given in Table 2. For population statistics, N_p refers to a population pruned of outlier values.

Fig. 6. (A–E) Examples of quartz arenite boulders sampled for cosmogenic ^{10}Be surface-exposure dating. **(F)** Deformed lacustrine sediments exposed in the Bocatoma terminal moraine, confirming that the glacier margin actively advanced into the valley bottom prior to depositing the moraine.

Fig. 7. Temporal reconstructions of (Top) ΔELA, (Middle) ΔT, and (Bottom) % length change for the three Cocuy glaciers during the Lateglacial period, early Holocene, and late Holocene. ΔT values are based upon the ELA reconstructions reported in Table 3.

Figure 1

Click here to access/download;Figure;Figure 1.jpg

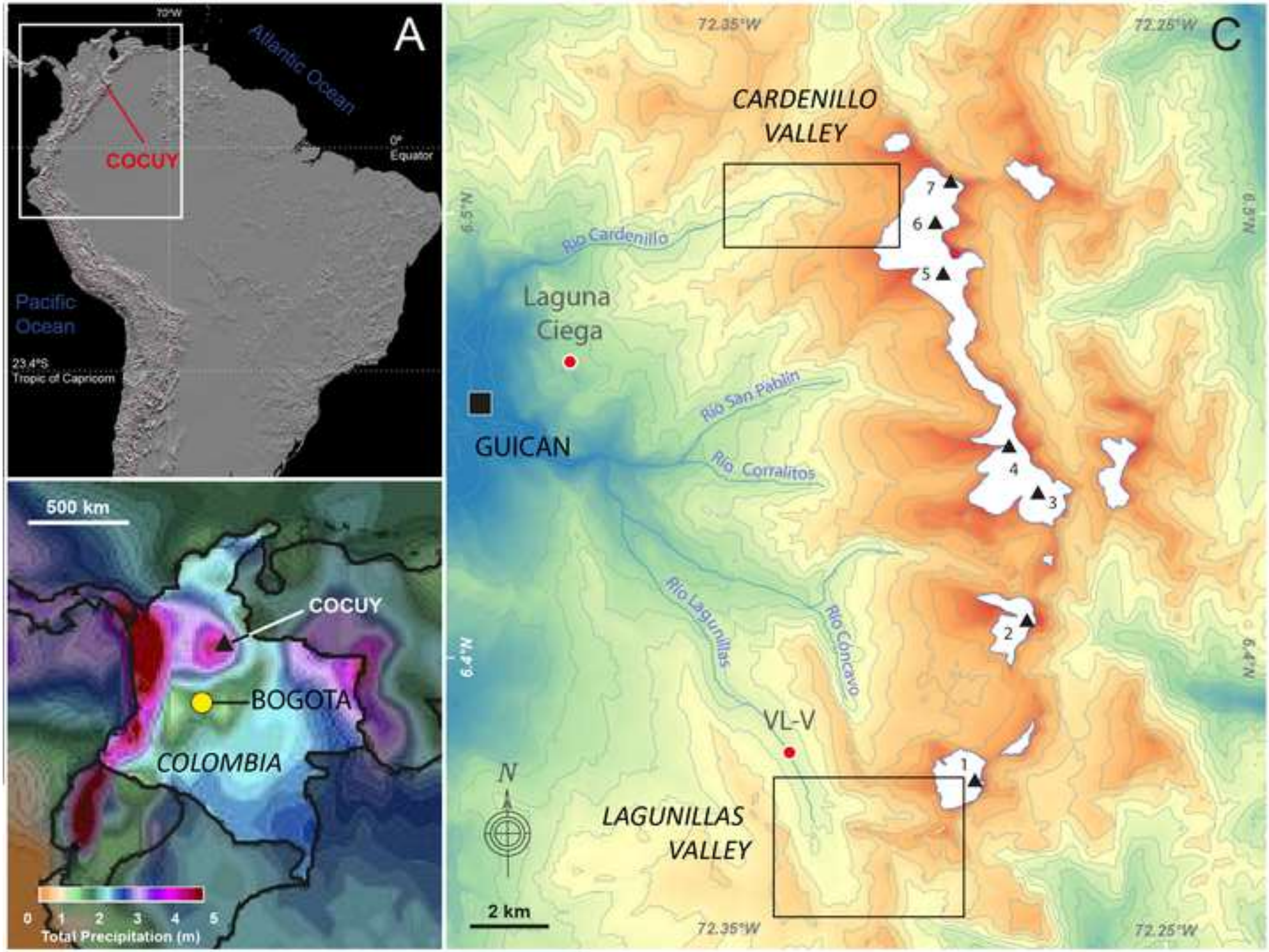

Figure 2

Click here to access/download;Figure;Figure 2.jpg

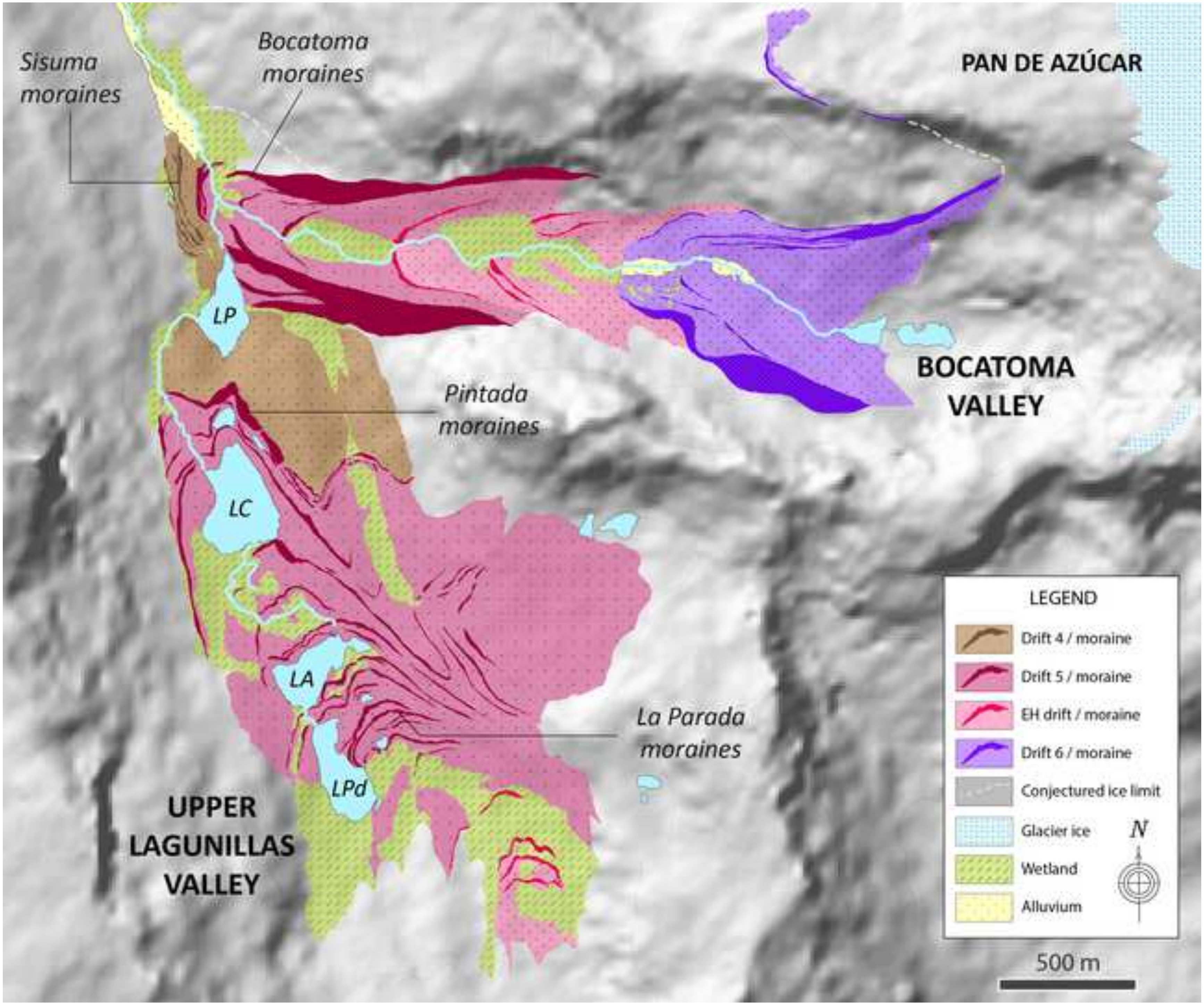

Figure 3

Click here to access/download;Figure;Figure 3-01-01.jpg

Figure 4 Click here to access/download;Figure;Figure 4.jpg

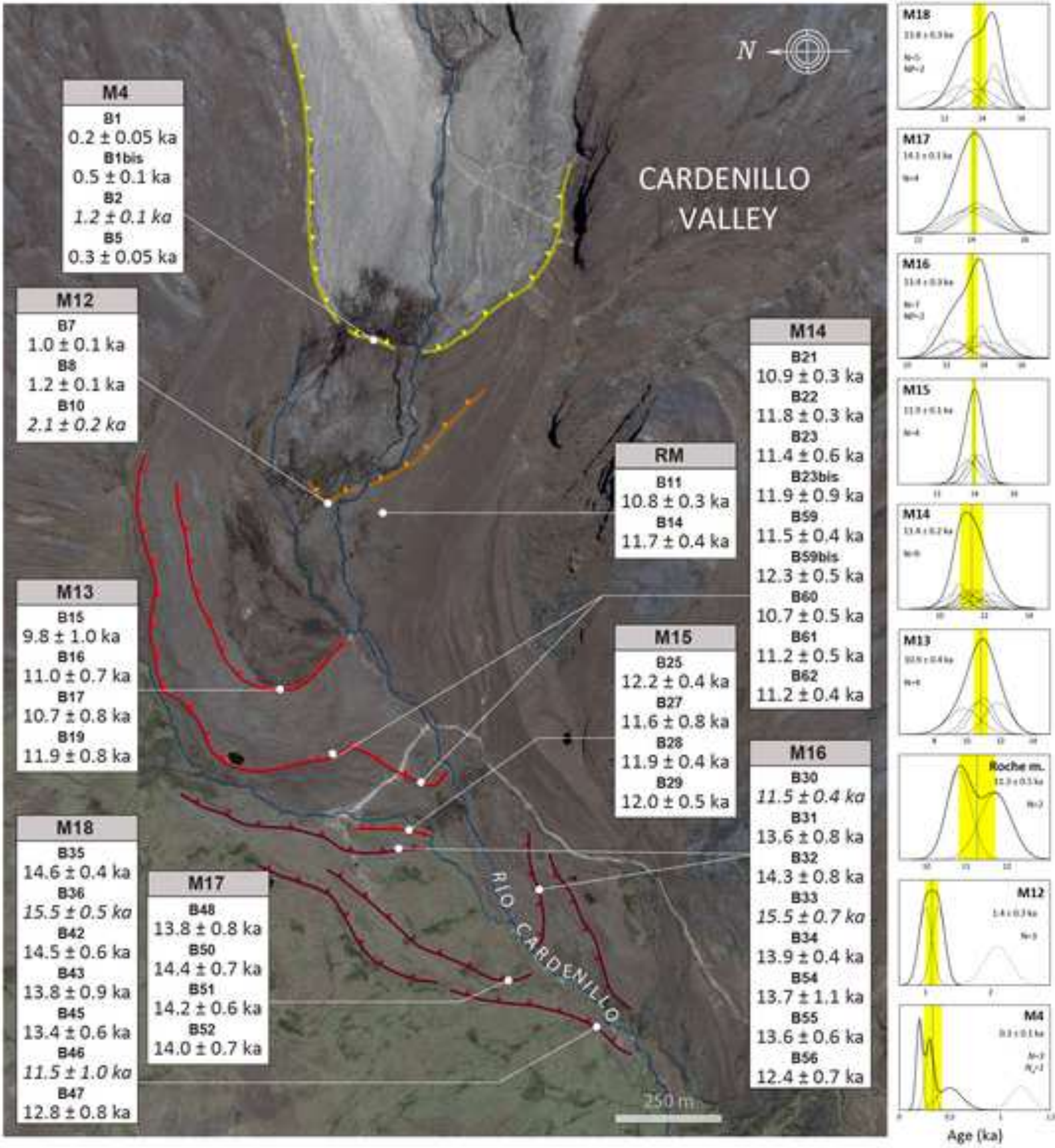

Figure 5

Click here to access/download;Figure;Figure 5.jpg

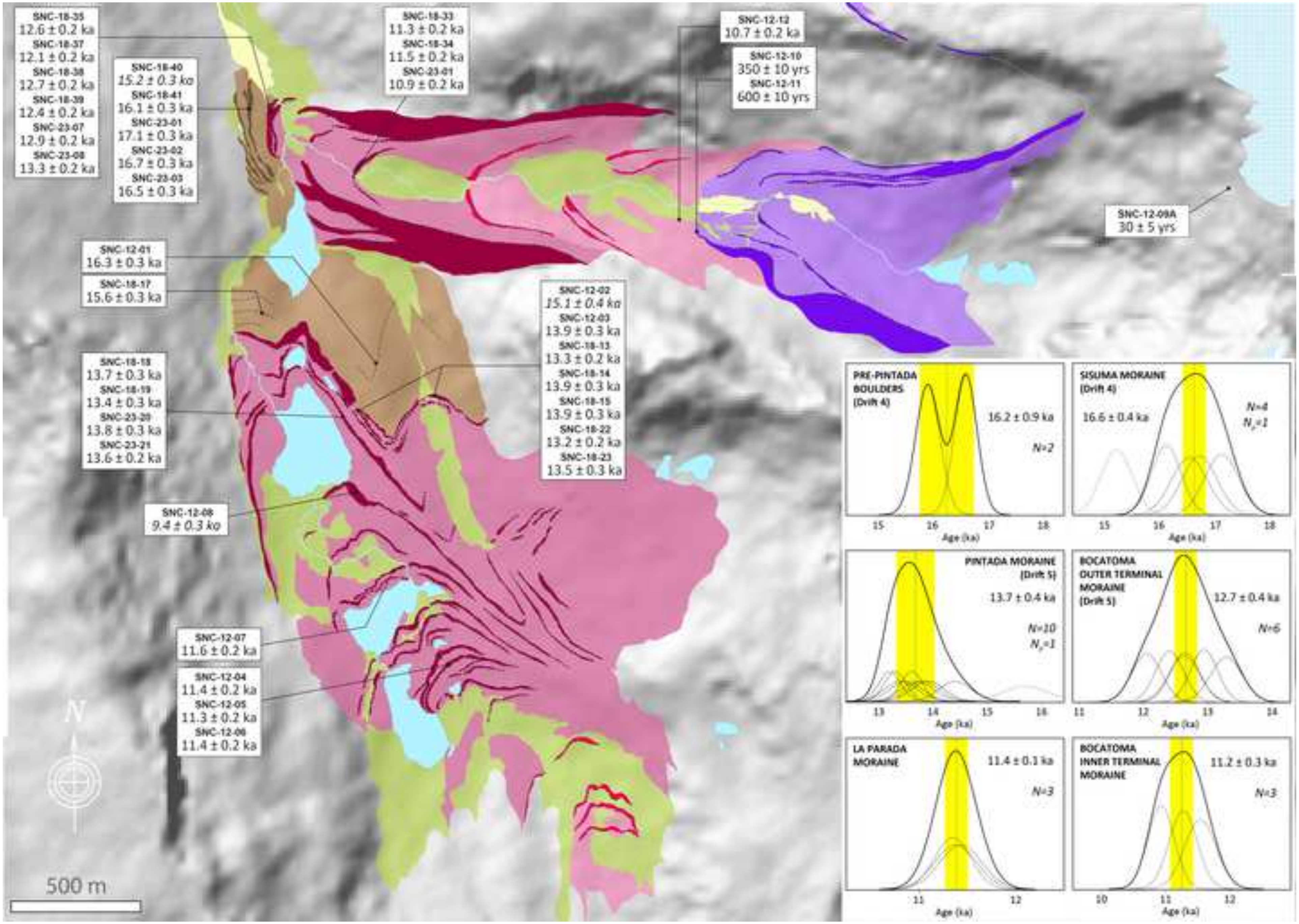

Figure 6

Click here to access/download;Figure;Figure 6-01.jpg

Figure 7

Click here to access/download;Figure;Figure 7.jpg

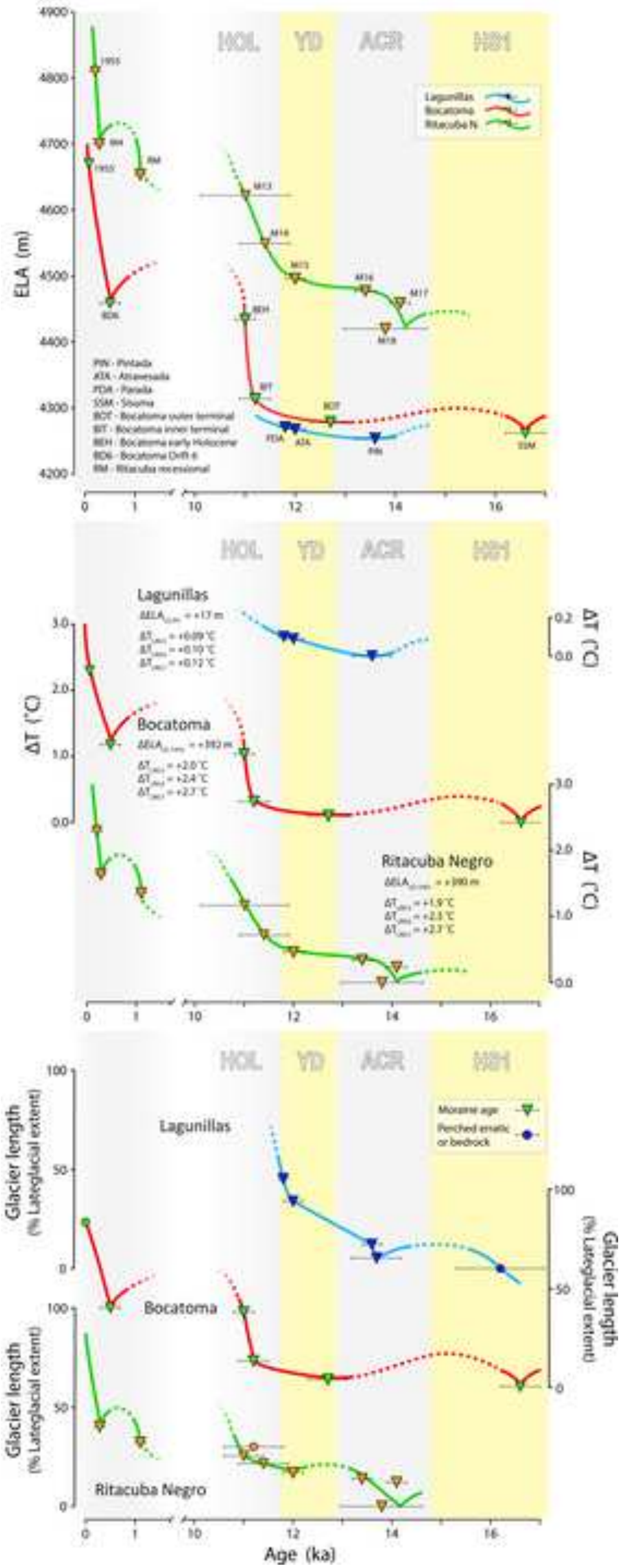

Table 1. ^{10}Be surface-exposure sample details and nuclide data for Lagunillas and Bocatoma samples. All measurements were made relative to the 07KNSTD AMS standard, which is dilution 01-5-4 from Nishiizumi et al. (2007), with a known ratio of 2850 x 10^{-15}. Shielding corrections were calculated using the UW topographic shielding calculator (https://stoneage.ice-d.org/math/skyline/skyline_in.html).

Landform	Sample ID	CAMS ID	Lat.	Long.	Elevation (m)	Sample thickness (cm)	Density (g/cm^{-2})	Shielding	Quartz weight (g)	^{9}Be added (μg)	10Be/9Be ±1σ (10^{-13}) [a]	[^{10}Be] ± 1σ (10^{5}) (atoms/g quartz) [b]
Lagunillas												
Pre-Pintada	SNC-12-01	BE37330	6.36190	-72.3350	4010	1.0	2.7	0.990	5.0765	0.206	1.68 ± 0.03	4.53 ± 0.09
	SNC-18-17	BE50415	6.36000	-72.3313	4048	3.0	2.7	0.987	7.2155	0.189	2.47 ± 0.05	4.32 ± 0.08
Pintada moraine	SNC-12-02	BE37331	6.35853	-72.3314	4059	0.5	2.7	0.990	5.0191	0.208	1.57 ± 0.04	4.32 ± 0.11
	SNC-12-03	BE37332	6.35782	-72.3309	4068	1.0	2.7	0.990	5.0781	0.207	1.47 ± 0.03	3.97 ± 0.09
	SNC-18-13	BE50293	6.35912	-72.3293	4045	1.1	2.7	0.977	7.0381	0.206	2.00 ± 0.04	3.71 ± 0.07
	SNC-18-14	BE50414	6.35878	-72.3301	4051	1.3	2.7	0.972	7.0019	0.206	2.20 ± 0.04	3.86 ± 0.07
	SNC-18-15	BE50286	6.35828	-72.3304	4075	2.1	2.7	0.985	7.0037	0.207	2.09 ± 0.04	3.94 ± 0.07
	SNC-18-18	BE50416	6.35895	-72.3325	4048	1.5	2.7	0.990	7.0206	0.195	2.09 ± 0.04	3.87 ± 0.07
	SNC-18-19	BE50287	6.35909	-72.3326	4046	1.8	2.7	0.990	7.0016	0.194	2.03 ± 0.04	3.77 ± 0.08
	SNC-18-20	BE50288	6.35909	-72.3326	4046	1.3	2.7	0.990	7.0623	0.196	2.11 ± 0.04	3.91 ± 0.07
	SNC-18-21	BE50289	6.35972	-72.3329	4044	1.6	2.7	0.990	7.0000	0.198	2.03 ± 0.03	3.83 ± 0.06
	SNC-18-22	BE50290	6.36057	-72.3333	4040	2.0	2.7	0.991	6.9940	0.196	1.98 ± 0.04	3.71 ± 0.07
	SNC-18-23	BE50291	6.36028	-72.3331	4043	1.5	2.7	0.991	7.0137	0.198	2.02 ± 0.04	3.81 ± 0.07
Cuadrada moraine	SNC-12-08	BE40318	6.35545	-72.3314	4057	1.3	2.7	0.990	7.0650	0.210	1.34 ± 0.03	2.66 ± 0.05
La Atravesada mor.	SNC-12-07	BE40317	6.35362	-72.3306	4057	1.6	2.7	0.990	7.0156	0.210	1.64 ± 0.03	3.28 ± 0.05
La Parada moraine	SNC-12-04	BE40314	6.35053	-72.3289	4083	2.2	2.7	0.990	7.0163	0.211	1.63 ± 0.03	3.26 ± 0.06
	SNC-12-05	BE40315	6.35012	-72.3297	4076	2.0	2.7	0.990	7.0031	0.211	1.61 ± 0.03	3.23 ± 0.03
	SNC-12-06	BE40316	6.34935	-72.3295	4071	0.6	2.7	0.990	7.0530	0.211	1.64 ± 0.03	3.27 ± 0.03
Sisuma moraine	SNC-18-40	BE50299	6.36735	-72.3350	3963	1.2	2.7	0.985	7.0165	0.196	2.20 ± 0.04	4.11 ± 0.08
	SNC-18-41	BE50300	6.36739	-72.3351	3964	1.3	2.7	0.986	7.0060	0.197	2.32 ± 0.04	4.36 ± 0.07
	SNC-23-01	BE54103	6.36874	-72.3353	3968	2.0	2.7	0.978	5.9238	0.211	1.93 ± 0.04	4.59 ± 0.08
	SNC-23-02	BE54104	6.36809	-72.3351	3970	2.6	2.7	0.980	6.1388	0.209	1.96 ± 0.04	4.46 ± 0.09
	SNC-23-03	BE54105	6.36782	-72.3351	3978	2.8	2.7	0.980	6.0925	0.210	1.92 ± 0.04	4.42 ± 0.09
Outer Bocatoma moraine	SNC-18-35	BE50296	6.36584	-72.3341	3966	2.1	2.7	0.982	7.0475	0.197	1.81 ± 0.04	3.39 ± 0.07
	SNC-18-37	BE50297	6.36740	-72.3344	3956	2.8	2.7	0.983	6.9992	0.197	1.72 ± 0.03	3.21 ± 0.06
	SNC-18-38	BE50419	6.36729	-72.3343	3956	3.2	2.7	0.983	7.0188	0.195	1.81 ± 0.03	3.36 ± 0.06
	SNC-18-39	BE50298	6.36706	-72.3345	3959	1.4	2.7	0.983	7.0141	0.193	1.82 ± 0.03	3.36 ± 0.06
	SNC-23-07	BE54106	6.36753	-72.3344	3978	1.6	2.7	0.983	5.9468	0.206	1.51 ± 0.03	3.51 ± 0.06
	SNC-23-08	BE54107	6.36708	-72.3345	3978	2.8	2.7	0.983	5.9177	0.209	1.51 ± 0.03	3.57 ± 0.07
Inner Bocatoma moraine	SNC-18-32	BE50294	6.36638	-72.3316	4025	2.7	2.7	0.985	7.0084	0.197	1.65 ± 0.03	3.10 ± 0.06
	SNC-18-33	BE50295	6.36635	-72.3317	4042	1.3	2.7	0.985	7.0010	0.197	1.71 ± 0.04	3.21 ± 0.07

	SNC-18-34	BE50417	6.36631	-72.3317	4025	1.3	2.7	0.987	7.0471	0.196	1.64 ± 0.03	3.05 ± 0.06
Early Holocene err.	SNC-12-12	BE40311	6.36469	-72.3217	4180	4.4	2.7	0.970	30.1050	0.209	6.61 ± 0.02	3.07 ± 0.07
Drift 5 moraine	SNC-12-10	BE40309	6.36445	-72.3209	4202	2.0	2.7	0.970	30.1040	0.209	0.22 ± 0.01	0.10 ± 0.003
	SNC-12-11	BE40310	6.36445	-72.3209	4202	4.9	2.7	0.970	30.1570	0.209	0.39 ± 0.01	0.18 ± 0.004
Ice-proximal BR	SNC-12-09A	BE40603	6.36569	-72.3040	4723	2.3	2.7	0.980	100.6700	0.125	0.12 ± 0.01	0.01 ± 0.001

[a] Beryllium ratios reported with no blank correction.

[b] Sample concentrations reported with blank correction.

Table 2. Cosmogenic ^{10}Be surface-exposure ages and internal [external] uncertainties calculated using the Quelccaya Ice Cap production rate (Kelly *et al*., 2013) and three current scaling models. Italics denote outliers.

Landform	Sample ID	St (ka)	Lm (ka)	LSDn (ka)
Lagunillas				
Pre-Pintada	SNC-12-01	**16.3 ± 0.3** [1.2]	15.0 ± 0.3 [1.1]	15.4 ± 0.3 [1.1]
	SNC-18-17	**15.6 ± 0.3** [1.1]	14.5 ± 0.3 [1.1]	14.9 ± 0.3 [1.1]
Pintada	SNC-12-02	**15.1 ± 0.4** [1.1]	14.1 ± 0.4 [1.1]	14.5 ± 0.4 [1.1]
	SNC-12-03	**13.9 ± 0.3** [1.0]	13.2 ± 0.3 [1.0]	13.5 ± 0.3 [1.0]
	SNC-18-13	**13.3 ± 0.2** [1.0]	12.8 ± 0.2 [0.9]	13.0 ± 0.2 [0.9]
	SNC-18-14	**13.9 ± 0.3** [1.0]	13.2 ± 0.2 [1.0]	13.5 ± 0.3 [1.0]
	SNC-18-15	**13.9 ± 0.3** [1.0]	13.2 ± 0.2 [1.0]	13.5 ± 0.3 [1.0]
	SNC-18-18	**13.7 ± 0.3** [1.0]	13.1 ± 0.2 [1.0]	13.3 ± 0.2 [1.0]
	SNC-18-19	**13.4 ± 0.3** [1.0]	12.8 ± 0.3 [1.0]	13.1 ± 0.3 [1.0]
	SNC-18-20	**13.8 ± 0.3** [1.0]	13.1 ± 0.2 [1.0]	13.4 ± 0.3 [1.0]
	SNC-18-21	**13.6 ± 0.2** [1.0]	13.0 ± 0.2 [0.9]	13.2 ± 0.2 [1.0]
	SNC-18-22	**13.2 ± 0.2** [1.0]	12.7 ± 0.2 [0.9]	12.9 ± 0.2 [0.9]
	SNC-18-23	**13.5 ± 0.3** [1.0]	12.9 ± 0.2 [0.9]	13.1 ± 0.2 [1.0]
Cuadrada	SNC-12-08	*9.4 ± 0.3 [0.7]*	*9.5 ± 0.2 [0.7]*	*9.6 ± 0.2 [0.7]*
La Atravesada	SNC-12-07	**11.6 ± 0.2** [0.8]	11.2 ± 0.2 [0.8]	11.3 ± 0.2 [0.8]
La Parada	SNC-12-04	**11.4 ± 0.2** [0.8]	11.1 ± 0.2 [0.8]	11.2 ± 0.2 [0.8]
	SNC-12-05	**11.3 ± 0.2** [0.8]	11.2 ± 0.2 [0.8]	11.2 ± 0.2 [0.8]
	SNC-12-06	**11.4 ± 0.2** [0.8]	11.1 ± 0.2 [0.8]	11.2 ± 0.2 [0.8]
Bocatoma				
Sisuma	SNC-18-40	*15.2 ± 0.3 [1.1]*	*14.1 ± 0.3 [1.0]*	*14.6 ± 0.3 [1.1]*
	SNC-18-41	**16.1 ± 0.3** [1.2]	14.9 ± 0.3 [1.1]	15.3 ± 0.3 [1.1]
	SNC-23-01	**17.1 ± 0.3** [1.2]	15.5 ± 0.3 [1.1]	16.2 ± 0.3 [1.2]
	SNC-23-02	**16.7 ± 0.3** [1.2]	15.2 ± 0.3 [1.1]	15.8 ± 0.3 [1.2]
	SNC-23-03	**16.5 ± 0.3** [1.2]	15.1 ± 0.3 [1.1]	15.7 ± 0.3 [1.2]
Outer Bocatoma	SNC-18-35	**12.6 ± 0.2** [0.9]	12.0 ± 0.2 [0.9]	12.4 ± 0.2 [0.9]
	SNC-18-37	**12.1 ± 0.2** [0.9]	11.5 ± 0.2 [0.8]	11.8 ± 0.2 [0.9]
	SNC-18-38	**12.7 ± 0.2** [0.9]	12.0 ± 0.2 [0.9]	12.2 ± 0.2 [0.9]
	SNC-18-39	**12.4 ± 0.2** [0.9]	11.8 ± 0.2 [0.9]	12.2 ± 0.2 [0.9]
	SNC-23-07	**12.9 ± 0.2** [0.9]	12.4 ± 0.2 [0.9]	12.7 ± 0.2 [0.9]
	SNC-23-08	**13.3 ± 0.2** [1.0]	12.8 ± 0.2 [0.9]	13.0 ± 0.2 [0.9]
Inner Bocatoma	SNC-18-32	**11.3 ± 0.2** [0.8]	11.0 ± 0.2 [0.8]	11.2 ± 0.2 [0.8]
	SNC-18-33	**11.5 ± 0.2** [0.8]	11.2 ± 0.2 [0.8]	11.3 ± 0.2 [0.8]
	SNC-18-34	**10.9 ± 0.2** [0.8]	10.8 ± 0.2 [0.8]	10.9 ± 0.2 [0.8]
Early Holocene	SNC-12-12	**10.7 ± 0.2** [0.8]	10.6 ± 0.2 [0.8]	10.7 ± 0.2 [0.8]
Drift 5 moraine	SNC-12-10	**0.3 ± 0.01** [0.03]	0.3 ± 0.01 [0.03]	0.3 ± 0.01 [0.03]
	SNC-12-11	**0.6 ± 0.01** [0.05]	0.7 ± 0.01 [0.05]	0.6 ± 0.01 [0.05]
Ice-proximal BR	SNC-12-09A	**03 ± 0.002** [0.003]	0.02 ± 0.002 [0.002]	0.03 ± 0.002 [0.002]
Cardenillo				
M18	B35	**14.6 ± 0.4** [1.1]	13.7 ± 0.4 [1.1]	14.1 ± 0.4 [1.1]
	B36	*15.5 ± 0.5 [1.2]*	*14.4 ± 0.5 [1.1]*	*14.9 ± 0.5 [1.1]*
	B42	**14.5 ± 0.6** [1.2]	13.7 ± 0.6 [1.1]	14.0 ± 0.6 [1.1]
	B43	**13.8 ± 0.9** [1.3]	13.1 ± 0.8 [1.3]	13.4 ± 0.9 [1.3]
	B45	**13.4 ± 0.6** [1.1]	12.8 ± 0.6 [1.1]	13.0 ± 0.6 [1.1]
	B46	*11.5 ± 1.0 [1.3]*	*11.2 ± 1.0 [1.3]*	*11.3 ± 1.0 [1.3]*
	B47	**12.8 ± 0.8** [1.2]	12.2 ± 0.8 [1.2]	12.5 ± 0.8 [1.2]
M17	B48	**13.8 ± 0.8** [1.2]	13.9 ± 0.8 [1.2]	13.4 ± 0.8 [1.2]
	B50	**14.4 ± 0.7** [1.2]	13.6 ± 0.6 [1.1]	13.9 ± 0.6 [1.2]
	B51	**14.2 ± 0.6** [1.2]	13.4 ± 0.6 [1.1]	13.7 ± 0.6 [1.2]
	B52	**14.1 ± 0.7** [1.2]	13.3 ± 0.7 [1.2]	13.6 ± 0.7 [1.2]
M16	B30	*11.5 ± 0.4 [0.9]*	*11.2 ± 0.4 [0.9]*	*11.3 ± 0.4 [0.9]*
	B31	**13.6 ± 0.8** [1.3]	13.0 ± 0.8 [1.2]	13.2 ± 0.8 [1.2]
	B32	**14.3 ± 0.8** [1.3]	13.5 ± 0.7 [1.2]	13.8 ± 0.7 [1.2]
	B33	*15.5 ± 0.7 [1.3]*	*14.4 ± 0.6 [1.2]*	*14.8 ± 0.6 [1.2]*
	B34	**13.9 ± 0.4** [1.1]	13.2 ± 0.4 [1.0]	13.5 ± 0.4 [1.0]
	B54	**13.7 ± 1.1** [1.5]	13.0 ± 1.0 [1.4]	13.3 ± 1.1 [1.4]
	B55	**13.6 ± 0.6** [1.1]	13.0 ± 0.6 [1.1]	13.2 ± 0.6 [1.1]
	B56	**12.4 ± 0.7** [1.1]	11.7 ± 0.7 [1.1]	12.1 ± 0.7 [1.1]

	B57	**12.4 ± 0.8** [1.2]	11.8 ± 0.7 [1.1]	12.1 ± 0.7 [1.1]
M15	B25	**12.2 ± 0.4** [1.0]	11.6 ± 0.4 [0.9]	11.9 ± 0.4 [0.9]
	B27	**11.6 ± 0.8** [0.9]	11.2 ± 0.5 [0.9]	11.4 ± 0.5 [0.9]
	B28	**11.9 ± 0.4** [0.9]	11.4 ± 0.4 [0.9]	11.6 ± 0.4 [0.9]
	B29	**12.1 ± 0.5** [1.0]	11.5 ± 0.4 [0.9]	11.7 ± 0.5 [0.9]
M14	B21	**10.9 ± 0.3** [0.8]	10.8 ± 0.3 [0.8]	10.9 ± 0.3 [0.8]
	B22	**11.8 ± 0.3** [0.9]	11.3 ± 0.3 [0.9]	11.5 ± 0.4 [0.9]
	B23	**11.4 ± 0.6** [1.0]	11.1 ± 0.6 [1.0]	11.2 ± 0.6 [1.0]
	B23bis	**11.9 ± 0.9** [1.2]	11.4 ± 0.9 [1.2]	11.6 ± 0.9 [1.2]
	B59	**11.5 ± 0.4** [0.9]	11.2 ± 0.4 [0.9]	11.3 ± 0.4 [0.9]
	B59bis	**12.4 ± 0.5** [1.0]	11.7 ± 0.5 [1.0]	12.0 ± 0.5 [1.0]
	B60	**10.7 ± 0.5** [0.9]	10.6 ± 0.5 [0.9]	10.7 ± 0.5 [0.9]
	B61	**11.2 ± 0.5** [0.9]	11.0 ± 0.5 [0.9]	11.1 ± 0.5 [0.9]
	B62	**11.2 ± 0.4** [0.9]	11.0 ± 0.4 [0.9]	11.1 ± 0.4 [0.9]
M13	B15	**9.8 ± 1.0** [1.2]	9.9 ± 1.0 [1.2]	10.0 ± 1.0 [1.2]
	B16	**11.0 ± 0.7** [1.0]	10.9 ± 0.7 [1.0]	11.0 ± 0.7 [1.0]
	B17	**10.7 ± 0.8** [1.1]	10.7 ± 0.8 [1.1]	10.8 ± 0.8 [1.1]
	B19	**11.9 ± 0.8** [1.1]	11.4 ± 0.7 [1.1]	11.6 ± 0.8 [1.1]
Roche moutonnée	B11	**10.8 ± 0.3** [0.8]	10.7 ± 0.3 [0.8]	10.8 ± 0.3 [0.8]
	B14	**11.7 ± 0.4** [0.9]	11.2 ± 0.3 [0.9]	11.4 ± 0.4 [0.9]
M12	B7	**1.1 ± 0.1** [0.1]	1.2 ± 0.1 [0.2]	1.1 ± 0.1 [0.1]
	B8	**1.2 ± 0.1** [0.2]	1.4 ± 0.2 [0.2]	1.3 ± 0.1 [0.2]
	B10	*2.1 ± 0.2 [0.3]*	*2.6 ± 0.3 [0.3]*	*2.4 ± 0.2 [0.3]*
M4	B1	**0.2 ± 0.03** [0.03]	0.2 ± 0.03 [0.03]	0.2 ± 0.03 [0.03]
	B1bis	**0.5 ± 0.1** [0.1]	0.5 ± 0.1 [0.1]	0.5 ± 0.1 [0.1]
	B2	*1.2 ± 0.1 [0.2]*	*1.4 ± 0.2 [0.2]*	*1.3 ± 0.1 [0.2]*
	B5	**0.3 ± 0.04** [0.4]	0.2 ± 0.03 [0.4]	0.3 ± 0.03 [0.4]

Table 3. Reconstructed ELAs for dated landforms in the Lagunillas, Bocatoma, and Cardenillo drainages calculated using a range of AAR and BR values.

Landform	AAR	ELA (m)	BR	ELA (m)
Sisuma moraine (16.6 ± 0.4 ka)	0.6	**4405**	2	**4399**
	0.7	**4337**	3	**4363**
	0.8	**4262**	4	**4338**
	0.9	**4161**	5	**4319**
Bocatoma outer moraine (12.7 ± 0.4 ka)	0.6	**4420**	2	**4418**
	0.7	**4356**	3	**4382**
	0.8	**4279**	4	**4357**
	0.9	**4186**	5	**4338**
Bocatoma inner moraine (11.2 ± 0.3 ka)	0.6	**4437**	2	**4443**
	0.7	**4386**	3	**4411**
	0.8	**4314**	4	**4389**
	0.9	**4240**	5	**4380**
Bocatoma early Holocene (11.0 ± 0.2 ka)	0.6	**4527**	2	**4547**
	0.7	**4487**	3	**4518**
	0.8	**4434**	4	**4499**
	0.9	**4357**	5	**4484**
Bocatoma Drift 6 moraine (0.5 ± 0.2 ka)	0.6	**4526**	2	**4552**
	0.7	**4493**	3	**4528**
	0.8	**4458**	4	**4511**
	0.9	**4403**	5	**4499**
Bocatoma 1955 extent	0.6	**4744**	2	**4756**
	0.7	**4707**	3	**4735**
	0.8	**4671**	4	**4721**
	0.9	**4626**	5	**4710**
Pintada moraine (13.7 ± 0.4 ka)	0.6	**4325**	2	**4311**
	0.7	**4295**	3	**4294**
	0.8	**4254**	4	**4281**
	0.9	**4196**	5	**4271**
La Atravesada moraine (12.0 ± 0.2 ka)	0.6	**4320**	2	**4319**
	0.7	**4296**	3	**4305**
	0.8	**4268**	4	**4294**
	0.9	**4229**	5	**4286**
La Parada moraine (11.8 ± 0.05 ka)	0.6	**4337**	2	**4330**
	0.7	**4305**	3	**4314**
	0.8	**4271**	4	**4303**
	0.9	**4229**	5	**4294**
M18 moraine (13.8 ± 0.3 ka)	0.6	**4719**	2	**4644**
	0.7	**4620**	3	**4589**
	0.8	**4420**	4	**4550**
	0.9	**4280**	5	**4520**
M17 moraine (13.8 ± 0.8 ka)	0.6	**4715**	2	**4657**
	0.7	**4618**	3	**4605**
	0.8	**4459**	4	**4568**
	0.9	**4305**	5	**4540**
M16 moraine (13.3 ± 0.8 ka)	0.6	**4714**	2	4662
	0.7	**4621**	3	4612
	0.8	**4477**	4	4577
	0.9	**4324**	5	4549
M15 moraine	0.6	**4722**	2	**4677**

(11.9 ± 0.2 ka)	0.7	**4632**	3	**4627**
	0.8	**4497**	4	**4592**
	0.9	**4335**	5	**4564**
M14 moraine (11.4 ± 0.5 ka)	0.6	**4753**	2	**4704**
	0.7	**4682**	3	**4653**
	0.8	**4549**	4	**4616**
	0.9	**4337**	5	**4587**
M13 moraine (10.9 ± 0.4 ka)	0.6	**4770**	2	**4734**
	0.7	**4712**	3	**4691**
	0.8	**4622**	4	**4660**
	0.9	**4425**	5	**4635**
Cardenillo late Holocene (1.1 ± 0.1 ka)	0.6	**4794**	2	**4760**
	0.7	**4736**	3	**4718**
	0.8	**4653**	4	**4687**
	0.9	**4474**	5	**4663**
Cardenillo Drift 6 moraine (0.3 ± 0.2 ka)	0.6	**4815**	2	**4788**
	0.7	**4762**	3	**4754**
	0.8	**4699**	4	**4729**
	0.9	**4577**	5	**4709**
Cardenillo 1955 extent	0.6	**4903**	2	**4920**
	0.7	**4858**	3	**4893**
	0.8	**4809**	4	**4875**
	0.9	**4751**	5	**4862**

Quelccaya Ice Cap production rate input data from Kelly *et al.* (2015).

Data selected from ice-D calibration site for v.3 of the UW online calculator. Dataset includes 12 of the 15 tota

Cut and paste data below into the online calculator: https://hess.ess.washington.edu/math/v3/v3_

K2015-Q-40 -13.94420 -70.89360 4853 std 1.5 2.29 0.9980 0.00e+00 0;
K2015-Q-40 true_t HUANCANE2A 12200 560;
K2015-Q-40 Be-10 quartz 5.452e+05 1.342e+04 KNSTD;
K2015-Q-42 -13.94500 -70.89290 4857 std 1.6 2.29 0.9960 4.51e-04 0;
K2015-Q-42 true_t HUANCANE2A 12200 560;
K2015-Q-42 Be-10 quartz 5.673e+05 9.690e+03 KNSTD;
K2015-Q-43 -13.94370 -70.89530 4844 std 1.5 2.29 0.9990 4.51e-04 0;
K2015-Q-43 true_t HUANCANE2A 12200 560;
K2015-Q-43 Be-10 quartz 5.533e+05 1.361e+04 KNSTD;
K2015-Q-44 -13.94500 -70.89540 4849 std 2.0 2.29 1.0000 0.00e+00 0;
K2015-Q-44 true_t HUANCANE2A 12200 560;
K2015-Q-44 Be-10 quartz 5.540e+05 1.364e+04 KNSTD;
K2015-Q-46 -13.94630 -70.89240 4863 std 0.9 2.29 1.0000 4.51e-04 0;
K2015-Q-46 true_t HUANCANE2A 12200 560;
K2015-Q-46 Be-10 quartz 5.716e+05 1.403e+04 KNSTD;
K2015-Q-47 -13.94630 -70.89210 4865 std 2.1 2.29 1.0000 4.51e-04 0;
K2015-Q-47 true_t HUANCANE2A 12200 560;
K2015-Q-47 Be-10 quartz 5.714e+05 1.158e+04 07KNSTD;
K2015-Q-48 -13.94610 -70.89270 4862 std 3.4 2.29 0.9980 4.51e-04 0;
K2015-Q-48 true_t HUANCANE2A 12200 560;
K2015-Q-48 Be-10 quartz 5.896e+05 1.350e+04 07KNSTD;
K2015-Q-49 -13.94580 -70.89350 4851 std 5.1 2.29 1.0000 4.51e-04 0;
K2015-Q-49 true_t HUANCANE2A 12200 560;
K2015-Q-49 Be-10 quartz 5.863e+05 1.107e+04 KNSTD;
K2015-Q-83 -13.94400 -70.89230 4856 std 3.2 2.29 0.9750 0.00e+00 0;
K2015-Q-83 true_t HUANCANE2A 12200 560;
K2015-Q-83 Be-10 quartz 4.954e+05 9.280e+03 07KNSTD;
K2015-Q-135 -13.94680 -70.88620 4863 std 2.3 2.29 0.9990 4.51e-04 0;
K2015-Q-135 true_t HUANCANE2A 12200 560;
K2015-Q-135 Be-10 quartz 5.159e+05 1.150e+04 07KNSTD;
K2015-Q-136 -13.94630 -70.88650 4866 std 2.3 2.29 0.9930 4.51e-04 0;
K2015-Q-136 true_t HUANCANE2A 12200 560;
K2015-Q-136 Be-10 quartz 4.993e+05 1.196e+04 07KNSTD;
K2015-Q-137 -13.94570 -70.88550 4870 std 2.1 2.29 0.9990 4.51e-04 0;
K2015-Q-137 true_t HUANCANE2A 12200 560;
K2015-Q-137 Be-10 quartz 5.433e+05 1.020e+04 07KNSTD;

l samples from the Huancance IIa moraines; three samples (Q-40a, 44a, and 83a) were omitted by the from the

cal_in.html

e original calibration and thus are not included here (see section 4.2.1 in Kelly et al. (2015)).

UW v.3 online calculator input data for all samples reported in Table 1

Sample groupings below correspond to those given in Table 1

Sample ID	Latitude	Longitude	Elevation	Atmosphere	Thickness
Pre-Pintada					
SNC-12-01	6.3619	-72.3350	4010	std	1.0
SNC-18-17	6.3600	-72.3313	4048	std	3.0
Pintada					
SNC-12-02	6.3585	-72.3314	4059	std	0.5
SNC-12-03	6.3578	-72.3309	4068	std	1.0
SNC-18-13	6.3591	-72.3293	4045	std	1.1
SNC-18-14	6.3588	-72.3301	4051	std	1.3
SNC-18-15	6.3583	-72.3304	4075	std	2.1
SNC-18-18	6.3590	-72.3325	4048	std	1.5
SNC-18-19	6.3591	-72.3326	4046	std	1.8
SNC-18-20	6.3591	-72.3326	4046	std	1.3
SNC-18-21	6.3597	-72.3329	4044	std	1.6
SNC-18-22	6.3606	-72.3333	4040	std	2.0
SNC-18-23	6.3603	-72.3331	4043	std	1.5
Cuadrada					
SNC-12-08	6.3555	-72.3314	4057	std	1.3
La Atravesada					
SNC-12-07	6.3536	-72.3306	4057	std	1.6
La Parada					
SNC-12-04	6.3505	-72.3289	4083	std	2.2
SNC-12-05	6.3501	-72.3297	4076	std	2.0
SNC-12-06	6.3494	-72.3295	4071	std	0.6
Sisuma					
SNC-18-40	6.3674	-72.3350	3963	std	1.2
SNC-18-41	6.3674	-72.3351	3964	std	1.3
SNC-23-01	6.3687	-72.3353	3968	std	1.9
SNC-23-02	6.3681	-72.3351	3970	std	2.6
SNC-23-03	6.3678	-72.3351	3978	std	2.8
Outer Bocatoma					
SNC-18-35	6.3658	-72.3341	3966	std	2.1
SNC-18-37	6.3674	-72.3344	3956	std	2.8
SNC-18-38	6.3673	-72.3343	3956	std	3.2
SNC-18-39	6.3671	-72.3345	3959	std	1.4
SNC-23-07	6.3675	-72.3344	3978	std	1.6
SNC-23-08	6.3671	-72.3345	3978	std	2.8
Inner Bocatoma					
SNC-18-32	6.3664	-72.3316	4025	std	2.7
SNC-18-33	6.3664	-72.3317	4024	std	1.3
SNC-18-34	6.3663	-72.3317	4025	std	1.3
Early Holocene					
SNC-12-12	6.3647	-72.3217	4180	std	4.4
Drift 5					

SNC-12-10	6.3645	-72.3209	4202	std	2.0
SNC-12-11	6.3645	-72.3209	4202	std	4.9
Ice-proximal BR					
SNC-12-09A	6.3657	-72.3040	4723	std	2.3
M18					
B35	6.5069	-72.3489	3998	std	3.5
B36	6.5068	-72.3489	3998	std	3
B42	6.5076	-72.3482	4024	std	4
B43	6.5075	-72.3483	4020	std	3
B45	6.5072	-72.3486	4005	std	4
B46	6.5070	-72.3487	3999	std	2
B47	6.5070	-72.3487	4000	std	3
M17					
B48	6.5088	-72.3468	4046	std	2
B50	6.5088	-72.3468	4049	std	1.5
B51	6.5089	-72.3468	4051	std	2.5
B52	6.5089	-72.3468	4050	std	2
M16					
B30	6.5081	-72.3451	4059	std	2.5
B31	6.5081	-72.3451	4059	std	2.5
B32	6.5081	-72.3449	4060	std	2
B33	6.5082	-72.3448	4065	std	2.5
B34	6.5082	-72.3448	4064	std	2
B54	6.5109	-72.3442	4086	std	2.5
B55	6.5109	-72.34425	4086	std	2
B56	6.5110	-72.34422	4088	std	3
B57	6.51105	-72.34439	4087	std	2.5
M15					
B25	6.50981	-72.34429	4059	std	5.5
B27	6.50987	-72.34428	4062	std	3
B28	6.50987	-72.34428	4062	std	5.5
B29	6.5097	-72.34430	4058	std	5.5
M14					
B21	6.51	-72.34272	4079	std	1
B22	6.50995	-72.3427	4078	std	2
B23	6.50988	-72.34263	4076	std	3
B23bis	6.50988	-72.34263	4076	std	3
B59	6.51256	-72.34179	4175	std	2.5
B59bis	6.51256	-72.34179	4175	std	2.5
B60	6.51254	-72.34176	4175	std	3
B61	6.51251	-72.34173	4175	std	2
B62	6.51247	-72.34176	4175	std	2
M13					
B15	6.51245	-72.34066	4139	std	2
B16	6.51252	-72.34072	4135	std	3
B17	6.51259	-72.34079	4137	std	2
B19	6.51308	-72.34072	4133	std	2

Roche Moutonnée					
B11	6.51119	-72.33775	4137	std	3
B14	6.51119	-72.33775	4137	std	2
M12					
B7	6.51184	-72.3369	4147	std	3.5
B8	6.51194	-72.33698	4147	std	4
B10	6.51207	-72.33718	4142	std	1.5
M4					
B1	6.50956	-72.33397	4209	std	2
B1bis	6.50956	-72.33397	4209	std	2
B2	6.50961	-72.33398	4203	std	2
B5	6.51063	-72.33369	4203	std	2.5

Density	Shielding	Erosion	Collection year	Sample ID	Nuclide
2.7	0.990	0	2012;	SNC-12-01	Be-10
2.7	0.987	0	2018;	SNC-18-17	Be-10
2.7	0.990	0	2012;	SNC-12-02	Be-10
2.7	0.990	0	2012;	SNC-12-03	Be-10
2.7	0.977	0	2018;	SNC-18-13	Be-10
2.7	0.972	0	2018;	SNC-18-14	Be-10
2.7	0.985	0	2018;	SNC-18-15	Be-10
2.7	0.990	0	2018;	SNC-18-18	Be-10
2.7	0.990	0	2018;	SNC-18-19	Be-10
2.7	0.990	0	2018;	SNC-18-20	Be-10
2.7	0.990	0	2018;	SNC-18-21	Be-10
2.7	0.991	0	2018;	SNC-18-22	Be-10
2.7	0.991	0	2018;	SNC-18-23	Be-10
2.7	0.990	0	2012;	SNC-12-08	Be-10
2.7	0.990	0	2012;	SNC-12-07	Be-10
2.7	0.990	0	2012;	SNC-12-04	Be-10
2.7	0.990	0	2012;	SNC-12-05	Be-10
2.7	0.990	0	2012;	SNC-12-06	Be-10
2.7	0.985	0	2018;	SNC-18-40	Be-10
2.7	0.986	0	2018;	SNC-18-41	Be-10
2.7	0.978	0	2023;	SNC-23-01	Be-10
2.7	0.978	0	2023;	SNC-23-02	Be-10
2.7	0.978	0	2023;	SNC-23-03	Be-10
2.7	0.982	0	2018;	SNC-18-35	Be-10
2.7	0.985	0	2018;	SNC-18-37	Be-10
2.7	0.985	0	2018;	SNC-18-38	Be-10
2.7	0.988	0	2018;	SNC-18-39	Be-10
2.7	0.985	0	2023;	SNC-23-07	Be-10
2.7	0.985	0	2023;	SNC-23-08	Be-10
2.7	0.985	0	2018;	SNC-18-32	Be-10
2.7	0.985	0	2018;	SNC-18-33	Be-10
2.7	0.987	0	2018;	SNC-18-34	Be-10
2.7	0.970	0	2012;	SNC-12-12	Be-10

2.7	0.970	0	2012;	SNC-12-10	Be-10
2.7	0.970	0	2012;	SNC-12-11	Be-10
2.7	0.980	0	2012;	SNC-12-09A	Be-10
2.7	0.993	0	2012;	B35	Be-10
2.7	0.993	0	2012;	B36	Be-10
2.7	0.996	0	2012;	B42	Be-10
2.7	0.995	0	2012;	B43	Be-10
2.7	0.994	0	2012;	B45	Be-10
2.7	0.992	0	2012;	B46	Be-10
2.7	0.994	0	2012;	B47	Be-10
2.7	0.995	0	2012;	B48	Be-10
2.7	0.995	0	2012;	B50	Be-10
2.7	0.993	0	2012;	B51	Be-10
2.7	0.996	0	2012;	B52	Be-10
2.7	0.993	0	2012;	B30	Be-10
2.7	0.991	0	2012;	B31	Be-10
2.7	0.992	0	2012;	B32	Be-10
2.7	0.994	0	2012;	B33	Be-10
2.7	0.993	0	2012;	B34	Be-10
2.7	0.995	0	2012;	B54	Be-10
2.7	0.995	0	2012;	B55	Be-10
2.7	0.994	0	2012;	B56	Be-10
2.7	0.993	0	2012;	B57	Be-10
2.7	0.994	0	2012;	B25	Be-10
2.7	0.994	0	2012;	B27	Be-10
2.7	0.994	0	2012;	B28	Be-10
2.7	0.993	0	2012;	B29	Be-10
2.7	0.989	0	2012;	B21	Be-10
2.7	0.990	0	2012;	B22	Be-10
2.7	0.989	0	2012;	B23	Be-10
2.7	0.989	0	2012;	B23bis	Be-10
2.7	0.996	0	2012;	B59	Be-10
2.7	0.996	0	2012;	B59bis	Be-10
2.7	0.996	0	2012;	B60	Be-10
2.7	0.996	0	2012;	B61	Be-10
2.7	0.996	0	2012;	B62	Be-10
2.7	0.987	0	2012;	B15	Be-10
2.7	0.987	0	2012;	B16	Be-10
2.7	0.986	0	2012;	B17	Be-10
2.7	0.988	0	2012;	B19	Be-10

2.7	0.985	0	2012;	B11	Be-10
2.7	0.985	0	2012;	B14	Be-10
2.7	0.986	0	2012;	B7	Be-10
2.7	0.989	0	2012;	B8	Be-10
2.7	0.988	0	2012;	B10	Be-10
2.7	0.976	0	2012;	B1	Be-10
2.7	0.976	0	2012;	B1bis	Be-10
2.7	0.976	0	2012;	B2	Be-10
2.7	0.984	0	2012;	B5	Be-10

Mineral	10Be atoms/g	1σ	AMS standard
quartz	4.53E+05	8.74E+03	07KNSTD;
quartz	4.32E+05	8.00E+03	07KNSTD;
quartz	4.32E+05	1.13E+04	07KNSTD;
quartz	3.97E+05	9.08E+03	07KNSTD;
quartz	3.71E+05	6.67E+03	07KNSTD;
quartz	3.86E+05	7.14E+03	07KNSTD;
quartz	3.94E+05	7.31E+03	07KNSTD;
quartz	3.87E+05	7.18E+03	07KNSTD;
quartz	3.77E+05	8.29E+03	07KNSTD;
quartz	3.91E+05	7.33E+03	07KNSTD;
quartz	3.83E+05	6.11E+03	07KNSTD;
quartz	3.71E+05	6.96E+03	07KNSTD;
quartz	3.81E+05	7.07E+03	07KNSTD;
quartz	2.66E+05	5.01E+03	07KNSTD;
quartz	3.28E+05	5.37E+03	07KNSTD;
quartz	3.26E+05	6.14E+03	07KNSTD;
quartz	3.23E+05	5.29E+03	07KNSTD;
quartz	3.27E+05	6.17E+03	07KNSTD;
quartz	4.11E+05	7.88E+03	07KNSTD;
quartz	4.36E+05	7.30E+03	07KNSTD;
quartz	4.59E+05	8.32E+03	07KNSTD;
quartz	4.46E+05	8.50E+03	07KNSTD;
quartz	4.42E+05	8.74E+03	07KNSTD;
quartz	3.39E+05	6.52E+03	07KNSTD;
quartz	3.21E+05	6.17E+03	07KNSTD;
quartz	3.36E+05	5.98E+03	07KNSTD;
quartz	3.36E+05	5.94E+03	07KNSTD;
quartz	3.51E+05	5.75E+03	07KNSTD;
quartz	3.57E+05	6.66E+03	07KNSTD;
quartz	3.10E+05	5.96E+03	07KNSTD;
quartz	3.21E+05	6.77E+03	07KNSTD;
quartz	3.05E+05	5.65E+03	07KNSTD;
quartz	3.07E+05	6.83E+03	07KNSTD;

quartz	1.01E+04	3.31E+02	07KNSTD;
quartz	1.80E+04	4.03E+02	07KNSTD;
quartz	1.01E+03	7.02E+01	07KNSTD;
quartz	3.98E+05	1.22E+04	NIST_27900;
quartz	4.24E+05	1.48E+04	NIST_27900;
quartz	3.99E+05	1.65E+04	NIST_27900;
quartz	3.82E+05	2.44E+04	NIST_27900;
quartz	3.64E+05	1.59E+04	NIST_27900;
quartz	3.18E+05	2.70E+04	NIST_27900;
quartz	3.50E+05	2.22E+04	NIST_27900;
quartz	3.91E+05	2.18E+04	NIST_27900;
quartz	4.08E+05	1.89E+04	NIST_27900;
quartz	3.99E+05	1.80E+04	NIST_27900;
quartz	3.98E+05	2.04E+04	NIST_27900;
quartz	3.25E+05	1.00E+04	NIST_27900;
quartz	3.83E+05	2.35E+04	NIST_27900;
quartz	4.06E+05	2.18E+04	NIST_27900;
quartz	4.39E+05	1.89E+04	NIST_27900;
quartz	3.96E+05	1.27E+04	NIST_27900;
quartz	3.93E+05	3.12E+04	NIST_27900;
quartz	3.92E+05	1.80E+04	NIST_27900;
quartz	3.53E+05	2.01E+04	NIST_27900;
quartz	3.56E+05	2.16E+04	NIST_27900;
quartz	3.36E+05	1.22E+04	NIST_27900;
quartz	3.28E+05	1.34E+04	NIST_27900;
quartz	3.29E+05	1.14E+04	NIST_27900;
quartz	3.32E+05	1.27E+04	NIST_27900;
quartz	3.14E+05	9.87E+03	NIST_27900;
quartz	3.36E+05	1.03E+04	NIST_27900;
quartz	3.23E+05	1.63E+04	NIST_27900;
quartz	3.37E+05	2.63E+04	NIST_27900;
quartz	3.45E+05	1.11E+04	NIST_27900;
quartz	3.69E+05	1.59E+04	NIST_27900;
quartz	3.18E+05	1.51E+04	NIST_27900;
quartz	3.37E+05	1.38E+04	NIST_27900;
quartz	3.36E+05	1.31E+04	NIST_27900;
quartz	2.87E+05	2.91E+04	NIST_27900;
quartz	3.20E+05	1.93E+04	NIST_27900;
quartz	3.13E+05	2.31E+04	NIST_27900;
quartz	3.47E+05	2.27E+04	NIST_27900;

quartz	3.13E+05	1.01E+04	NIST_27900;
quartz	3.40E+05	1.05E+04	NIST_27900;
quartz	3.05E+04	3.21E+03	NIST_27900;
quartz	3.49E+04	3.85E+03	NIST_27900;
quartz	6.18E+04	6.22E+03	NIST_27900;
quartz	7.37E+03	8.51E+02	NIST_27900;
quartz	1.39E+04	3.65E+03	NIST_27900;
quartz	3.66E+04	3.88E+03	NIST_27900;
quartz	7.66E+03	1.06E+03	NIST_27900;